UNIVERSITY *of York*

This is a repository copy of *Incorporation of strontium in earthworm-secreted calcium carbonate granules produced in strontium-amended and strontium-bearing soil*.

White Rose Research Online URL for this paper:
https://eprints.whiterose.ac.uk/75431/

Version: Submitted Version

Article:

White Rose
university consortium
Universities of Leeds, Sheffield & York

eprints@whiterose.ac.uk
https://eprints.whiterose.ac.uk/

1   Incorporation of strontium in earthworm-secreted calcium carbonate granules

2   produced in strontium-amended and strontium-bearing soil

3

4   L. Brinza[a,*], P.D. Quinn[a], P.F. Schofield[b], J.F.W. Mosselmans[a], M.E. Hodson[c,1]

5

6   [a] Diamond Light Source Ltd., Harwell Science and Innovation Campus, Chilton, Didcot,

7   OX11 0DE, UK

8   [b] Mineral and Planetary Sciences, Department of Earth Sciences, Natural History Museum,

9   Cromwell Road, London SW7 5BD, UK

10   [c] Soil Research Centre, Dept. Geography and Environmental Science, School of Human and

11   Environmental Sciences, University of Reading, Whiteknights, Reading, RG6 6DW, UK

12   * Corresponding author email address: loredana.brinza@diamond.ac.uk (Loredana Brinza)

13   +44 (0)1235 778517

14

15   Running head: Sr in earthworm granules

16

17

18

19

20

21

22

23

24

25

26   1. Present Address: Environment Department, University of York, Heslington, York, YO10

27   5DD, United Kingdom

28

29 **Abstract**

30 This paper investigates the incorporation of Sr into biomineralized calcium carbonate

31 granules secreted by the earthworm *Lumbricus terrestris.* Experiments were conducted

32 using an agricultural soil amended with $Sr(NO_3)_2$ to give concentrations in the range 50 - 500

33 mg kg^{-1} Sr and a naturally Sr-rich, Celestine-bearing soil containing up to 11 000 mg kg^{-1} Sr.

34 Granule production rates were in the range 0.26 – 2.3 mg_{CaCO3} earthworm^{-1} day^{-1}; they

35 showed no relationship with soil or soil solution Sr concentration but decreased with

36 decreasing pH. Strong relationships exist ($r^2 \geq 0.8$, $p \leq 0.01$) between the Sr concentrations

37 and Sr / Ca ratios of the granules and those of the soil, soil solution and earthworms. The

38 highest bulk Sr concentration we recorded in the calcium carbonate granules was 5.1 wt%

39 Sr whilst electron microprobe analysis recorded spot concentrations of up to 4.3 wt % Sr. X-

40 ray diffraction and X-ray absorption spectroscopy indicate that the majority of the calcium

41 carbonate is present as Sr-bearing calcite with trace amounts of Sr-bearing vaterite also

42 being present. The granules produced in the Sr-amended soils concentrated Sr relative to

43 Ca from the bulk soil and the earthworms. This suggests that earthworm secreted calcium

44 carbonate may be significant in the cycling of ^{90}Sr released into soils via nuclear accidents or

45 leakage from nuclear waste storage facilities.

46

47 **1. INTRODUCTION**

48

49   The incorporation of Sr (and other elements) into calcite and other calcium carbonate

50 phases has been, and continues to be, the subject of much research in the geochemical

51 community (e.g. Bracco et al., 2012; Tertre et al., 2012; DePaolo, 2011; Tang et al., 2008;

52 Lakshtanov and Stipp, 2007; Nehrke et al., 2007; Finch and Allison, 2007; Gabitov and

53 Watson, 2006; Elzinga and Reeder, 2002; Fujita et al., 2004; Parkman et al., 1998; Pingitore

54 et al., 1992; Stipp and Hochella, 1991; Tesoriero and Pankow, 1996). Some of the research

55 is driven by the potential for calcite to immobilise contaminants, particularly ^{90}Sr (e.g. Riley et

56 al., 1992; Achal et al. 2012; Perdrial et al., 2011; Spycher et al., 2009; Barkouki et al., 2011;

57 Fujita et al., 2010; Tertre et al., 2012). Additionally, the potential use of Sr/Ca ratios in

58 biominerals and speleothems for the reconstruction of past environments is also the subject

59 of numerous studies (e.g. Finch and Allison, 2007; Wassenburg et al., 2012; Sinclair et al.,

60 2012; Bluszcz et al., 2009; Fairchild et al, 2000, Dissard et al., 2010a, 2010b; Stoll et al.,

61 2002). This paper is concerned with Sr partitioning into earthworm-secreted calcite;

62 understanding this system may have important implications for site remediation and

63 environmental reconstruction.

64   Earthworms are perhaps best known for their role in the breakdown of organic

65 material and the mixing and aeration of soils (Edwards, 2004; Edwards and Bohlen, 1996).

66 However, many species of earthworm also synthesise calcium carbonate (Canti and

67 Piearce, 2003). The calcium carbonate is produced in the calciferous glands as micron-scale

68 spherites which, in many species, go on to coalesce and form millimetre scale granules

69 comprised predominantly of calcite, but also containing aragonite, vaterite and amorphous

70 calcium carbonate (e.g. Canti and Piearce, 2003; Gago-Duport et al., 2008; Lee et al., 2008).

71 The spherites and granules are secreted into the earthworm intestine and, from there, into

72 the soil. Carbon isotope studies of *L. terrestris* granules indicate that the carbon in the

73 granules comes from both carbon dioxide and consumed organic matter (Briones et al.,

74 2008; Canti, 2009). Granule production rates by the earthworm *Lumbricus terrestris* have

75 been linked to soil pH (Lambkin et al., 2011) but the function of the granules is still not clear

76 with suggested functions including Ca, CO_2 and pH regulation in body tissues and fluids

77 (Darwin, 1881, Robertson, 1936; Piearce, 1972).

78   It is well established that earthworms can accumulate metals when exposed to

79 contaminated or amended soils (e.g. Nahmani et al., 2007). We have shown (Fraser et al.,

80 2011) that, at least for Pb, metals can also accumulate in the calcium carbonate granules

81 secreted by earthworms in those soils; Pb was both structurally incorporated within the

82 calcite in the granules and also present as the Pb-carbonate cerrusite. The Pb-enriched

83 granules contained an unexpectedly large amount of aragonite, consistent with studies

84   which highlight the influence of various trace elements on calcium carbonate polymorph

85   transformations and stability (e.g., Sr, Mg, Zn, SO_4^{-2}) (Bots et al., 2011; Finch and Allison,

86   2007; Morse et al, 1997; Reis et al., 2008; Rodriguez-Blanco et al., 2011a; Wang et al.,

87   2012). Morgan et al. (2001, 2002) demonstrated that despite the chemical similarities

88   between Sr and Ca and the accumulation of Sr by earthworms exposed to Sr-rich soils,

89   earthworms are able to metabolically differentiate between Sr and Ca. Studies have shown

90   that the distribution coefficients for Sr incorporation in biosynthesised calcite are up to an

91   order of magnitude higher than values reported in natural and synthetic calcite (e.g. Fujita et

92   al., 2004; Morgan et al., 2001). Strontium 90 is produced by nuclear fission and is a

93   significant component of nuclear waste. It has been accidentally released into numerous

94   environments due to leaks from storage facilities (e.g. Hanford, USA, Thompson et al., 2010;

95   Oak Ridge, USA, Gu et al., 2005; Mayak, Russia, Standring et al., 2002 and Sellafield, UK,

96   Gray et al., 1995) and nuclear accidents (e.g. Fukushima Daiichi). Evidence suggests that

97   the partitioning of Sr into calcite (and other calcium carbonates) is related to environmental

98   variables such as temperature and CO_2 levels; consequently Sr/Ca ratios can be used as a

99   tool for reconstruction of past environments (Fairchild et al., 2000; Dissard et al., 2010a, b).

100   The aims of the current study were therefore to determine: 1) the extent to which Sr

101   would accumulate in the calcium carbonate produced by *L. terrestris* exposed to Sr-enriched

102   soils, 2) whether distribution coefficients for this incorporation were consistent with those

103   determined for inorganic systems, and 3) whether Sr incorporation impacted on granule

104   mineralogy. Our results are placed in the context of the potential of earthworm calcium

105   carbonate granules within the fields of contaminant immobilisation and environmental

106   reconstruction.

107

108

109   **2. METHODS**

110

111   **2.1. Earthworms and soils**

4

112   Clitellate *Lumbricus terrestris* were obtained from Recycle Works Ltd. (Ribchester,

113   PR3 3XJ, UK). They were kept for one week in a moist mixture of 1:2 by volume peat soil

114   and Kettering Loam (Boughton Loam and Turf Management, Kettering, Northamptonshire,

115   NN16 8UN, UK) prior to being used in the experiments.

116   Three arable soils were collected for the study, one, Hamble soil (HS) from near

117   Theale, Berkshire OS 164 (SU-618-702) and two Yate soils (Yate Soil High, YSH, and Yate

118   Soil Low, YSL) from the former celestine ($SrSO_4$) mining area of Yate, Bristol OS 172 (ST-

119   712-847) (Nickless et al., 1976).

120

2.2. Soil characterization

122   Prior to characterisation and experiment the soils were oven dried (at 40ºC) and

123   sieved to < 250 μm. Subsamples of the soil were dried at 105 °C to remove moisture

124   completely and all results are expressed on a per mass of 105 °C dried soil basis. Selected

125   soil properties are reported in Table 1. Soil water holding capacity (WHC) was determined

126   gravimetrically following ISO 11465:1993 (ISO, 1993). Soil pH in deionised water was

127   determined following BS ISO 10390:2005 (BSI 2005). Loss on ignition (LOI) was determined

128   following BS EN 15935 (BSI 2009) and used as a proxy for organic matter content

129   Soil elemental composition was determined by aqua regia digest following BS ISO

130   12914 (BSI, 2010) using an Anton Parr Multiwave 3000 microwave followed by analysis

131   using a Perkin Elmer Optima 7300 DV inductively coupled plasma – optical emission

132   spectrometer ICP-OES). For quality control, an internal reference soil material (SS50)

133   traceable to BCR-143R (Commission of the European Communities, Community Bureau of

134   Reference) and blanks were digested in triplicate. Recoveries were 93% for Ca and 107%

135   for Sr for SS50; repeated analysis of individual samples indicated a precision $\leq$ 0.5 % and

136   detection limits of less than 0.07 mg kg^{-1}.

137

2.3. Earthworm incubation experiments

139   Incubation experiments were carried out on the Hamble and Yate soils in a

140 temperature and ventilation controlled Memmert ICP 600 incubator set at 16 °C with minimal

141 ventilation. For the Hamble soil, incubations were carried out on unamended soil (HS) and

142 also Hamble soil to which solutions of anhydrous $Sr(NO_3)_2$ (Sigma-Aldrich, CAS 10042-76-9)

143 were added to give initial target Sr concentrations in soil of 50, 100, 150 and 500 mg Sr kg^{-1}

144 (denoted HS50, HS100, HS150 and HS500, respectively). Higher Sr concentrations (1000

145 and 4000 mg kg^{-1}) were also used but proved terminal to the earthworms and are not

146 reported here. Amended soils were digested in aqua regia and analysed by ICP-OES to

147 check concentrations. Incubation experiments were carried out in plastic containers

148 enclosed in perforated plastic bags. Each container held 300 mg oven dried soil mixed with

149 either deionised water or $Sr(NO_3)_2$ solution to give a water content of c. 60% of the WHC. An

150 individual *L. terrestris* was weighed and added into each soil sample. Five replicates were

151 run for each concentration.

152   After 28 days earthworms were removed from the soil, depurated for 48 hours

153 (Arnold and Hodson, 2007), digested by aqua regia and analysed for Sr and Ca by ICP-

154 OES. Detection limits and precision were as reported for the soil digestions. Soil pore water

155 was extracted overnight with 100 mm epoxy bodied MOM Rhizon samplers. pH was

156 measured with a Jenway 3510 pH meter; precision was 0.36 %. Solutions were then

157 acidified with 5% concentrated (≥69%) Sigma-Aldrich nitric acid ACS reagent grade,

158 ISO≥69% (CAS 7697-37-2) prior to analysis by ICP-OES for Ca and Sr. An in house 500 µg

159 kg^{-1} standard gave recoveries of 90 – 110 %. Detection limits were ≤ 0.017 mg kg^{-1} and

160 precision was < 2.2%. Soil sub-samples were taken from each incubation for pH

161 measurement (BSI, 2005). The remaining soil was sieved to 500 µm to recover the granules.

162 Granules from each replicate treatment were dried and pooled for weighing to determine

163 production rate expressed as mg CaCO$_3$/g worm/day prior to further characterization.

164   Two additional incubation experiments were carried out. In one, Hamble soil

165 amended to 500 mg Sr kg^{-1} was incubated but without any earthworm additions. No granules

166 were recovered from this incubation supporting the earthworm-derived origin of the granules.

167 In the second, granules recovered from our unamended Hamble soil experiment were added

168 to Hamble soil amended to 500 mg Sr kg^{-1} using Sr(NO$_3$)$_2$. After 28 days the granules were

169 characterised for chemical composition as described in Section 2.4.

170

171 **2.4. Granule characterization**

172   The majority of granules were dissolved in 5% nitric acid and analysed by ICP-OES.

173 The certified reference material dolomite BCS No386 was also digested following this

174 method and gave a recovery of 117% for Ca. Detection limits were $\leq$ 0.028 mg kg^{-1} with

175 precision of $\leq$ 1.3 %. Remaining granules were used in mineralogical and spatially resolved

176 chemical investigations.

177   Thin sections of the granules were produced by embedding the granules in EpoFIX

178 (Struers) resin and grinding to a thickness of 50-70 µm, that is, 25-35 µm either side of the

179 granule centre. The granule slices were then mounted on Chance Glass Ltd. glass slides

180 and mechanically polished using a 1 µm particle size corundum slurry.

181   Bulk granule mineralogy was assessed by combining information gleaned from X-ray

182 powder diffraction (XRD-NHM) on powdered granules and in-house, non-destructive X-ray

183 microdiffraction (µXRD-NHM) on the polished granule sections that were then used for

184 electron probe analysis and X-ray absorption spectroscopy. XRD-NHM data were collected

185 in reflection geometry using a Nonius PDS 120 powder diffraction system consisting of an

186 Inel curved, position sensitive detector (PSD) within a static beam-sample-detector

187 geometry. This system allows the simultaneous measurement of the diffracted X-ray

188 intensities at all angles of 2θ across 120º (Schofield et al., 2002). Cobalt Kα_1 radiation was

189 selected from the primary beam by a germanium 111 crystal monochromator with the X-ray

190 tube operating at 35 kV and 30 mA. Horizontal and vertical slits restricted the beam to a

191 height of 0.24 mm and width of 4.0 mm. Individual granules were powdered in an agate

192 pestle and mortar, mixed with acetone and thinly deposited on a circular sapphire substrate.

193 NIST silicon powder SRM640 and silver behenate were used as external standards;

194   calibration and data collection were performed using in house software Diffgrab™. Data

195   were collected for a minimum of 2000 s with samples spinning continuously in the plane of

196   the sample surface and with the sample surface at an angle of 4.0º to the incident beam.

197   μXRD-NHM data were collected using a Nonius PDS 120 powder diffraction system as

198   described above. In this case a 100 μm diameter beam was selected by a pinhole from a

199   300 μm diameter primary beam of Cu Kα radiation generated by a GeniX system with a

200   Xenocs FOX2D CU 10_30P mirror operating at 50 kV and 1 mA (Lambiv Dzemua et al.,

201   2012). Measurements were made in reflection geometry. The surface of the granule polished

202   section was brought into the focal point of the beam using a Zeiss Axio Cam MRc5 CCD

203   optical system. The footprint of the beam on the sample was 750-500 × 100 μm. During data

204   collection, the polished sections were spun continuously in the plane of the sample surface.

205   NIST silicon powder SRM640 and silver behenate were used as external standards;

206   calibration and data collection were performed using Diffgrab™ with data collection times of

207   at least 3000 s.

208   Elemental distribution within the granules was mapped using both electron probe

209   microanalysis (EPMA) and synchrotron based X-ray fluorescence (sXRF). EPMA element

210   maps were generated using a Cameca SX100 electron microprobe operating at 15 kV and

211   100 nA with the beam set to a spot size of 1 μm. Wavelength dispersive spectrometers

212   (WDS) were used to detect elements Ca, Sr, Mn, Mg and Fe while the elements Na, Al, Si,

213   P, S, Cl, K and Ti were detected using an energy dispersive spectrometer (EDS). Maps were

214   512 × 512 pixels with step sizes of 4-5 μm and dwell times of 180 – 200 ms.

215   Quantitative electron microprobe chemical analyses of the granules were performed

216   using a WDS Cameca SX100 microprobe operating with 10 kV accelerating voltage, 100 nA

217   beam current, and a spot size of ~20 μm. All elements were analysed using WDS and the

218   probe standards used were: calcite for Ca, celestine for Sr and S, $MnTiO_3$ for Mn, forsterite

219   for Mg, fayalite for Fe, jadeite for Na, corundum for Al, KBr for K, and wollastonite for Si,

220    $ScPO_4$ for P. The X-ray intensities were corrected using a standard PAP correction

221   procedure. Between 20 and 40 points were analysed on each granule along rim-core-rim line

222   profiles. The atomistic detection limits for Ca, Mg, Sr and Mn were 0.05, 0.02, 0.03 and 0.04

223   wt %, respectively, and the wt % oxide standard deviations for CaO, MgO, SrO and MnO

224   were 0.5, 0.02, 0.03 and 0.03, respectively.

225   The sXRF was performed on the microfocus beamline I18 at the Diamond Light

226   Source (Mosselmans et al., 2009) where sXRF maps were collected using a 9-element Ge

227   detector with the Si(111) cryogenically-cooled monochromator set to provide an incident X-

228   ray energy of 16500 eV. The beam-on-sample size was 5 × 5 μm. and maps were collected

229   with 30 μm steps. XRF data were processed in PyMCA 4.4.1 (Solé et al., 2007). sXRF maps

230   were used principally to determine suitable points for microfocus X-ray absorption

231   spectroscopy.

232

233   **2.4.1. Micro X-ray Absorption Spectroscopy (µXAS)**

234   µXAS was carried out on the thin sections of the granules using the microfocus

235   beamline I18 at the Diamond Light Source. μXAS was carried out on one granule each

236   extracted from HS150, HS500, YSL and YSH and two granules extracted from HS100. For

237   most of the granules two Ca K-edge XANES and Sr K-edge EXAFS spectra were collected

238   from the same point of interest at several different points. Recurrent spectra were compared

239   to check for any sign of beam damage. For all the spectra obtained no changes were seen in

240   these recurrent spectra. XAS data were processed in Athena (Ravel and Newville, 2005)

241   and Pyspline (Tenderholt and Quinn, 2009) and fitted using DL_Excurv (Tomic et al., 2004).

242   Sr K-edge spectra of relevant standards were recorded as follows: celestine

243   (collected from the Yate soil), $SrCO_3$ (Fisher Scientific), and $Sr(NO_3)_2$ (Fisher Scientific)

244   spectra were obtained in transmission mode using samples ground together with boron

245   nitride and pressed into pellets. Fluorescence data were collected from Sr-containing

246   aragonite (this sample is speleothem aragonite from Makapansgat Valley, South Africa and

247   was provided by Dr. A. Finch, University of St Andrews), calcite with Sr adsorbed onto it,

248 earthworm-produced calcium carbonate granules with Sr adsorbed onto them and vaterite

249 co-precipitated with Sr.

250   Calcite for the Sr adsorbed standard was synthesized following the method of

251 Rodriguez-Blanco et al. (2011b). The powder produced had a BET surface area of 0.99 m^2

252 g^{-1} whilst the granules had a BET surface area of 0.83 m^2 g^{-1}. One gram of either the

253 synthesised calcite or calcium carbonate granules recovered from our unamended Hamble

254 soil experiment was equilibrated in 50 mL of a pH 7.5 solution of $NaHCO_3$ and HCl at 20 °C

255 for 24 hours, the pH adjusted back to 7.5 and then Sr added as $Sr(NO_3)_2$ (Sigma-Aldrich,

256 CAS 10042-76-9) to give a solution concentration of 100 nM Sr per g calcite. After 24 hours

257 the adsorbent was collected via centrifugation.

258   Vaterite co-precipitated with Sr was made following the method of Bots (2012). A

259 solution of 100 mM $CaCl_2$ was rigorously mixed with a solution of 50 mM Na_2CO_3 and 1.25 M

260 Na_2SO_4 on a magnetic stirring plate. Sr was added to the $CaCl_2$ solution as $Sr(NO_3)_2$ to give

261 a concentration of 100 µM Sr. Vaterite precipitated instantly, was washed by filtration with

262 deionised water to remove sulphate and dried in isopropanol. The precipitate was shown to

263 be pure vaterite using XRD.

264   An attempt was made to synthesize standards of calcite co-precipitated with Sr

265 following the method of Gruzensky (1967). Solutions of $CaCl_2$ with $SrCl_2$ were prepared to

266 give final Sr concentrations in solution of 100 µM, 1 µM and 10 mM Sr. In each case

267 however the resulting precipitate was a mixture. For solutions of 100 µM, and 1 µM Sr the

268 calcite was precipitated with vaterite while the solution of 10 mM Sr produced calcite with

269 Ca-bearing strontianite and aragonite.

270   Ca K-edge XANES data were collected in fluorescence mode from the speleothem

271 aragonite and also synthetic vaterite stabilized with 4% sulphate (provided by Dr. P. Bots,

272 University of Leeds). As the Ca XANES data were collected in fluorescence mode the

273 spectra are distorted by self-absorption. Corrections can, in principle, be made for self

274 absorption and a basic example of such a correction is shown for Ca K-edge XANES from a

275 calcite single crystal in the Supplementary Information. In order to make an accurate self-

276   absorption correction, a knowledge of the density of the sample is required. As the granules

277   of this study have a mineralogy that may vary within the volume of sample analysed at each

278   point, this is not a feasible option. Consequently, no corrections have been applied to the Ca

279   K-edge XANES from the granules in this study, however, as all the spectra were recorded in

280   the same way comparisons between the spectra can be made.

281

282   **2.5. Statistics**

283   Statistical analysis was carried out using Sigma Stat 3.0.1 by SPSS. All data were checked

284   for normality using the Kolmogorov-Smirnov test before analysis and appropriate parametric

285   or non-parametric statistics used. Soil Sr concentrations were compared using Kruskall-

286   Wallis one way analysis of variance on ranks, changes in earthworm weight during the

287   course of the experiment by one way analysis of variance. Pearson and Spearman's rank

288   correlations were determined as appropriate for relationships between soil, soil solution,

289   earthworm and granule chemistry and granule production.

290

291   **3. RESULTS AND DISCUSSIONS**

292   **3.1. Soil solution**

293   Sr concentrations in the amended Hamble soils varied about the target values potentially

294   due to uncertainties in extraction efficiency and analysis. However, importantly for the

295   present study soils with significantly different Sr concentrations were produced (Table 1, $p \leq$

296   0.01). The low concentrations of Sr in the soil solution in the YSL and YSH soils relative to

297   the Sr amended Hamble soils (Table 1) reflects the sources of Sr in the soils, celestine in the

298   Yate soils (Nickless et al., 1976) and the more soluble $Sr(NO_3)_2$ in the Sr-amended Hamble

299   soil.

300   **3.2. Earthworm survival and chemistry**

301   No earthworms died over the duration of the experiment but they all lost weight.

302   Average weight loss was 6.4 ± 11.8 % of their body weight (n = 6 ± s.d.). There were no

303   significant differences in weight loss between soils or treatments ($p \geq 0.05$). Earthworm

304   chemistry is summarised in Table 2. The range of Sr concentrations is similar to that

305   reported for different species kept in soils collected from the Yate region by Morgan et al.

306   (2001, 2002) but Ca concentrations are up to an order of magnitude higher. This appears to

307   reflect the higher Ca concentrations in our soils compared to those in Morgan's study (1250

308   – 5540 mg kg^{-1}). Additionally Morgan et al. (2001) studied different species of earthworms,

309   three of which, *Aporrectodea caliginosa, Aporrectodea longa* and *Allolobophora chlorotica,*

310   have less well developed calciferous glands which produce far fewer granules (Canti and

311   Piearce, 2003) which may impact on Ca accumulation. The concentration of Sr accumulated

312   by earthworms, in this study, increased with the concentration of Sr in the soil ($r^2 = 0.92$, $p \leq$

313   0.05) and the soil solution ($r^2 = 0.88$, $p \leq 0.05$), but no correlation was found for Ca

314   supporting the conclusion of Morgan et al. (2001) that Ca uptake is regulated whilst Sr

315   uptake is not.

316   Similarly to Morgan et al. (2001) concentration factors calculated for earthworm body

317   loads using the bulk soil concentrations for Sr and Ca were 0.89 ± 0.42 and 1.14 ± 0.45

318   (mean ± s.d., n = 32), respectively. Distribution coefficients (D) for Sr and Ca were

319   calculated as the ratio of the Sr/Ca in the earthworm and Sr/Ca in the soil or soil solution and

320   are given in Table 3. On average values for earthworm distribution coefficients are 0.81 ±

321   0.31 and 0.51 ± 0.26 (mean ± s.d., n = 32) for partitioning between the earthworm and soil

322   and the earthworm and soil solution, respectively, indicating that if uptake and accumulation

323   is from the bulk soil there is no discrimination between Sr and Ca ($D \cong 1$) whereas if uptake

324   is from the metal in solution Ca is preferentially taken up ($D < 1$). For the earthworm – soil

325   distribution coefficients the unamended Hamble soil and the YSL soil have relatively low

326   values presumably reflecting the low Sr content of the unamended Hamble soil and the non-

327   bioavailable nature of the Sr in the YSL soil, respectively.

328   The earthworm – soil solution partition coefficient for YSH is higher than the other

329   values, possibly reflecting the relatively high Sr / Ca ratio of the YSH soil solution. Unlike the

330   findings of Morgan et al. (2001) there is no indication that Sr bioaccumulation decreases

331   relative to Ca at higher soil Ca concentrations. This may reflect the narrower range of Sr and

332   Ca concentrations in our study and the fact that the low Sr concentration soils were

333   amended with highly soluble (and therefore more bioavailable) $Sr(NO_3)_2$ whilst the high Sr

334   concentration soils contained the less soluble (and therefore less bioavailable) celestine.

335

336   **3.3. Granule production, bulk mineralogy and bulk chemistry**

337   Granule production rates (Table 2) were similar to those reported by Fraser et al.

338   (2011) in Pb amended artificial soils and by Lambkin et al. (2011) in agricultural soils . There

339   were no significant correlations between the Sr concentration of the soil or soil solution and

340   granule production rate. The lower production rate recorded for soil YSL is consistent with

341   the reduction in granule production with decreasing pH reported by Lambkin et al. (2011).

342   Analysis of bulk and micro XRD data shows that calcite is the main component of the

343   granules with vaterite often present as well (Table 4). Trace amounts of quartz were

344   identified in all the granules but no Sr-carbonate or Sr-sulphate phases such as strontianite,

345   carbocernaite or celestine were identified. The quartz is potentially incorporated within

346   granules during their transportation from the calciferous glands into oesophageal pouches

347   where the granules are stored before being excreted and where granules growth may still

348   occur (Lee et al., 2008).

349   The bulk concentrations of Sr and Ca in the granules as measured by ICP-OES are

350   reported in Table 2, where it can be seen that substantial levels of Sr are incorporated into

351   the calcium carbonate granules. The concentrations of Sr reported in the granules are high

352   but similar values have been reported in the literature. Concentrations of Sr in inorganically

353 produced calcite reported in the literature include 8505 mg kg^{-1} (Pingitore et al., 1992), 1477

354 mg kg^{-1} (Tang et al., 2008) and 1300 – 3500 mg kg^{-1} (Gabitov and Watson, 2006).

355 Concentrations of Sr in biogenic calcite are often higher, with reported concentrations

356 including 27 000 mg kg^{-1} in the common groundwater, gram-positive bacteria, *Bacillus*

357 *pasteurei*, (Warren et al., 2001, with vaterite also present) and up to 5000 mg kg^{-1} in

358 decapods (Veizer, 1983). EPMA of the granules confirmed the high Sr concentrations within

359 the granules (Table 4). For granules produced in the Hamble soils the granules with the

360 highest SrO levels (up to 5 wt% SrO or 4.3 wt % Sr) are those produced in the soils

361 amended to the highest concentration of Sr. The high concentrations of Sr may in part reflect

362 the crystallisation history of the predominantly calcite granules given that initially the calcium

363 carbonate is amorphous (e.g. Gago-Duport et al. 2008) and that amorphous calcium

364 carbonate can be preserved in the granules (e.g. Lee et al. 2008). Calcite that forms via

365 amorphous calcium carbonate can have elevated Mg concentrations (e.g. Radha et al.,

366 2012; Raz et al, 2000; Wang et al. 2012) and it is possible that similar effects occur for Sr

367 though we are not aware of any published studies on this subject. It should also be noted

368 that the bulk Mg concentrations in the granules are low ($\leq$ 31 mg kg^{-1}) and even narrow

369 bands of high Mg concentration (Table 4) are below the levels found in many biogenic

370 calcites or thought to represent maxima for calcite formed directly from solution rather than

371 from an amorphous precursor (e.g. Berner, 1975, Fernández-Díaz et al., 1996; Loste et al.,

372 2003)

373   In order to assess the potential for Sr adsorbing to granule surfaces post

374 secretion/excretion granules produced in unamended, Sr-free Hamble soil were placed in

375 Hamble soil amended to 500 mg Sr kg^{-1} for 28 days. Subsequent ICP-OES analyses

376 revealed that Sr levels associated with the granules increased from 345 mg kg^{-1} in the

377 control granules (Table 2) to 1370 mg kg^{-1}. In contrast Sr levels in granules produced by

378 earthworms in Hamble soil amended to 500 mg Sr kg^{-1} were 34200 mg kg^{-1} (Table 2). This

379   suggests that if Sr adsorption from the soil solution to the granule surface occurs then it only

380   accounts for a small fraction of the total Sr associated with the granules.

381   As described in detail by Fraser et al. (2011), in X-ray diffraction the calcite 104 peak

382   position is a good indicator of relative changes in the size of the calcite unit cell. Calcite 104

383   peak positions taken from bulk XRD data are reported in Table 4. In order to ensure that

384   these XRD measurements are compared with appropriate Sr levels in granule calcite, the

385   wt% SrO of each granule was estimated from the average wt% SrO value from EPMA point

386   analyses within a rim-core line profile of large calcite crystals making up the granules (Table

387   4) rather than using the Sr concentrations measured by ICP-OES (Table 2) which are

388   average values for a range of granules and which will therefore include Sr present in

389   vaterite; however the trends observed are the same regardless of which Sr data are used.

390   Figure 1 shows the calcite 104 peak position as a function of the estimated average wt%

391   SrO from EPMA analyses for the granules produced by earthworms in Hamble soils (and not

392   those produced in Yate soils for which there is no "control" specimen, i.e. granules produced

393   in an equivalent soil but with the absence of Sr). It can been seen that the calcite 104 peak

394   shifts to lower 2θ values as the Sr concentration in the granule calcite increases. A shift of

395   the calcite 104 peak to lower 2θ values is indicative of an increasing unit cell size suggesting

396   that Sr, which is larger than Ca, is structurally incorporated by the calcite.

397   No aragonite was identified within any of the granules of this study, although the

398   study of Fraser et al. (2011) found granules comprising calcite and aragonite with no vaterite

399   being present. The current study used a natural soil amended with Sr and a natural Sr-rich

400   soil, whereas in the study of Fraser et al. (2011) the biogenic calcium carbonate granules

401   were produced by *L. terrestris* in artificial soil amended with Pb. This suggests that the

402   mineralogy of the calcium carbonate granules may be influenced by soil, consistent with

403   experiments on the inorganic calcium carbonate system (e.g. Bots et al., 2011; Finch and

404   Allison, 2007; Rodriguez-Blanco et al., 2011a). The production of mixtures of different

405   phases when we attempted to co-precipitate calcite with Sr using different concentrations of

406   Sr in solution to produce standards also supports this suggestion.

407   The Sr concentrations and the Sr/Ca ratio of the granules are strongly related ($r^2 \geq$

408   0.8, $p \leq 0.01$) to those of the soil, the soil solution and the earthworms. Distribution

409   coefficients (Table 3) suggest differences in the partitioning of Sr and Ca in the granules

410   between the Sr amended and naturally Sr-rich soils. The partitioning of Sr and Ca from the

411   soil and soil solution is mediated by the earthworm metabolic processes. As such the

412   distribution coefficients reported here cannot be fairly compared with distribution coefficients

413   for Sr and Ca partitioning in inorganic calcite precipitated from solution. However, the values

414   obtained are similar to that of 0.49 obtained for biogenic calcite produced by the bacterium

415   *Bacillus pasteurii,* (Fujita et al., 2004) and greater than many obtained for inorganic calcite

416   (e.g. 0.021 ± 0.003 by Tang et al., (2008) and up to 0.140 by Tesoriero and Pankow, (1996))

417   suggesting that earthworms, like bacteria (Warren et al., 2001), can more efficiently partition

418   Sr into calcite than inorganic processes. Indeed the distribution coefficients for partitioning

419   between the granules and bulk soils suggest that, for the Sr-amended soils, the granules

420   may preferentially concentrate Sr with the granule – earthworm partition coefficients for

421   these soils also suggesting the granules concentrate Sr relative to Ca compared to the

422   earthworm tissues. This finding is consistent with that of Morgan (1981) who found that Sr

423   injected directly into the coelomic cavity of *L. terrestris* in the form of $SrCl_2$ solution was

424   detected in the calciferous glands and spherites within the glands but not in the

425   chloragogenous tissue, an organ associated with the accumulation and metabolism of Ca.

426   The granule-soil and granule-soil solution partition coefficients are similar to those for

427   the earthworm-soil and earthworm–soil solution partition coefficients for the amended soils

428   but are substantially lower for the YSL and YSH soils. The granules have a relatively lower

429   Sr/Ca ratio than the earthworms in the YSL and YSH soils compared to the Sr amended

430   soils. This suggests that the accumulated Sr from the YSL and YSH soils is somehow

431   transported or metabolised differently to that accumulated from the amended soils or has a

432   different availability due to the soil chemistry. This would be expected given the different

433   forms of Sr present in the soils and is supported by the granule–earthworm partition

434   coefficients which show more partitioning of Sr relative to Ca in the granules compared to

435   the earthworms for the Sr amended soils. Despite the strong correlation between granule

436   and earthworm Sr, the granule-earthworm partition coefficients suggest that after Sr is

437   accumulated in the earthworm the partitioning of Sr into granules via the calciferous gland is

438   not a straight forward process dependent solely on Sr concentrations. For example the

439   distribution coefficient decreases with increasing earthworm Sr/Ca ($r^2 = 0.69$, $p \leq 0.05$)

440   perhaps suggesting that at higher Sr/Ca ratios there is preferential excretion of Sr preventing

441   its partitioning into the granules or that the transport path of Sr to the granules is saturated

442   (Chwodhury et al., 2000; Dodd, 1967). Alternatively this may reflect a precipitation rate

443   effect. In inorganic systems higher rates of calcite precipitation result in greater partitioning

444   of Sr into calcite (e.g. Nehrke et al., 2007; Tang et al., 2008; Tesoriero and Pankow, 1996;

445   Gabitov and Watson, 2006). Granule production rates are lower in the YSL and YSH soils

446   than in the HS soils perhaps suggesting a lower precipitation rate of calcite in the earthworm

447   calciferous glands and a consequent reduction in the partitioning of Sr into the calcite. This

448   also raises the possibility that the apparent preferential partitioning of Sr into biogenic calcite

449   compared to inorganic calcite discussed above may be due to precipitation kinetics.

450   The potential difference in partitioning of Sr to the granules between the amended

451   and non-amended soils suggests that further investigation is warranted. As such we carried

452   out spatially resolved studies to determine the compositional and crystallographic distribution

453   of Sr in the granules.

454

455   **3.4. Sr distribution within granules**

456   The internal structure of granules has been well described by Lee et al. (2008), and

457   in this study comprises two distinct types, with each type being found in granules extracted

458   from all the different treatments used in this study. The first type comprise a densely

459   compact aggregate of >30 μm carbonate crystals whose orientations appear to be consistent

460   (often radial) within individual layers (e.g. Fig. 2a). These granules are made up of only a few

461   distinct layers. The second type are silicate-inclusion rich and comprise several concentric

462   rings that are poorly linked together and are interspersed with large void spaces. The

463   carbonate crystals within these types of granules are generally smaller than those of the

464   more dense granules (e.g. Fig. 2b).

465   EPMA element maps of the granules from Hamble soils all show concentric

466   zoning of Sr, Mg and Mn. Similar zoning has been observed previously in granules produced

467   by *L. terrestris* in Hamble soil using cathodoluminescence and SEM imaging (Lee et. al.,

468   2008). There is no relationship between type of zoning and the different granule

469   morphologies described above. In general the concentric rings for the Sr were broad in

470   nature. However, there appears to be no consistency to the zoning within the granules either

471   across the study or within individual experiments / Sr amendments (Fig. 3). Some granules

472   from the Hamble soils showed Sr-rich cores and rims, some granules showed Sr-rich cores

473   and Sr-poor rims, and some granules showed Sr-poor cores with Sr-rich rims.

474   In contrast to the Sr, the concentric rings for Mg were generally very narrow and

475   distinct (Fig. 4) reflecting relatively large changes in Mg concentration (Table 4). This wide

476   range in Mg concentrations suggests that, unlike various other organisms (e.g. Bentov and

477   Erez, 2006; Lorens and Bender, 1977; Wang et al., 2012) there is no biotic control on the Mg

478   content of the earthworm-produced calcite. There appears to be no consistency between the

479   granules regarding the number, frequency or radial position of the Mg rich rings. The zoning

480   of the Mn within the granules was generally more diffuse than that for Sr and Mg, and the

481   concentric nature of the zoning showed broad bands rather than the ring structure displayed

482   by Mg. The Mn zoning patterns within the granules had far more consistency than for Sr and

483   Mg with granules from the same experiment displaying the same basic distribution of Mn-rich

484   and Mn-poor bands.

485   Statistical correlations between Ca, Sr, Mg and Mn were determined for both the

486   EPMA element maps and the quantitative point analyses across the rim-core-rim line

487   profiles. No significant correlations exist between any pair of elements.

488   Barker and Cox (2011) showed that laboratory synthesized inorganic calcite co-

489   precipitated with rare earth elements shows the same style of zoning as that observed in the

490   granules strongly suggesting that inorganic processes are responsible for the granule

491   zoning. The zoning is likely due to episodic elemental enrichment of the fluid surrounding the

492   granules and the subsequent incorporation of the enriched elements in the growing

493   granules. These fluctuations in concentration may be due to the composition of soil and soil

494   solution that the earthworm encounters at any given moment in time. Alternatively, or

495   additionally, they may be due to the incorporation of the trace elements into the granules

496   being more rapid than their replenishment at the granule growth front by diffusion through

497   the fluid in the calciferous gland; over time the concentration of the granule-incorporated

498   element would again increase in the fluid leading to its renewed incorporation into the

499   granule (Shore and Fowler, 1996). The apparent inconsistency in the zonation pattern for

500   granules within the same experiment may be due to changes over time in the chemistry of

501   the fluid from which the granules precipitate. In addition the elemental zoning may relate to

502   changes in the mechanism or pathway of the calcium carbonate formation reaction with

503   elemental enrichment being associated with the behaviour of potential precursor phases

504   such as amorphous calcium carbonate and/or vaterite.

505   The granules produced by *L. terrestris* in the Yate soil showed a different pattern of

506   elemental zoning. Sr was only present in a 5 – 60 μm wide zone around the rim of the YSL

507   granules and only present in ~200 μm diameter patches of microcrystalline calcium

508   carbonate in YSH granules. The zonation pattern for Mg within the YSL and YSH granules

509   was the same as that for the granules from Sr amended Hamble soil, while Mn showed no

510   zoning pattern in YSH and a small enriched rim in the YSL granules that correlated with the

511   zoning shown by Sr. These differences may reflect differences in the speciation of these

512   elements, and hence their availability for uptake, between the amended and naturally Sr-rich

513   soils. However, none-with-standing the large range of Mg values shown in the zoning

514   mitigating against a biological control over the Mg content of the calcite, the similarity in the

515   Mg zoning between the HS and YSL and YSH granules may somehow reflect the biological

516   origins of the granules.

517

518

519   **3.5. Sr and Ca μXAS of the granules**

520   **3.5.1. Ca K-edge XANES**

521   The Ca XANES spectra of the calcium carbonate standards and representative

522   spectra obtained from granules recovered from the experiments are shown in Figure 5. For

523   the HS granules we only present spectra obtained from a granule extracted from HS100 as

524   these are typical of the spectra obtained from the granules extracted from the other HS soils,

525   which themselves are presented in the Supplementary Information. Also given in the

526   Supplementary Information are spectra from other points analysed on granules extracted

527   from YSL and YSH.

528   The Ca XANES spectrum of the calcite standard has a pre-edge feature with two

529   peaks at 4.039 and 4.042 keV (marked "1" and "2" in Fig. 5) compared to the other

530   standards which show only one peak in the pre-edge. This pre-edge feature has previously

531   been highlighted by Lam et al. (2007) and Gebauer et al. (2010) and can be used to

532   differentiate calcite from vaterite or aragonite. The vaterite Ca-XANES spectrum in Fig. 5 is

533   similar to vaterite spectra previously reported in the literature (Bots, 2012; Gebauer et al.,

534   2010; Hayakawa et al., 2008; Lam et al., 2007). This spectrum has a single broad peak as a

535   pre-edge feature at 4.040 keV and two broad post edge peaks at 4.048 keV (marked "3" in

536   Fig. 5) and 4.056 keV (marked "4" in Fig. 5) and these two features can be used to

537   differentiate between vaterite and aragonite.

538   Typical Ca XANES spectra obtained from the granules are shown in Fig. 5. The majority of

539   the spectra (43 out of 45) obtained from granules recovered from the amended Hamble soils

540   from which granules were analysed (e.g. HS100 point A and B), all 6 spectra obtained from

541   granules recovered from YSL (e.g. YSL Point A) and 6 of the 10 spectra obtained from

542   granules recovered from YSH (e.g. YSH Point A) are similar to the calcite Ca K-edge

543   XANES spectrum (Fig. 5). The structural motif of the diagnostic pre- and post-edge features

544   at c. 4.048 eV and 4.060 eV are the same in all these specta, and thus confirm that these

545   granules are mostly calcitic in nature. Small differences in the post-edge region of these

546   spectra exist, specifically in the shape of the main peak and the broadness of the second

547   oscillation, which are similar to those described in our earlier study of Pb in earthworm

548   granules (Fraser et al., 2011). As described earlier, the granules predominantly comprise

549   large single crystals of calcite with respect to the size of the microbeam and thus each

550   spectrum is likely to be associated with one individual calcite crystal. Consequently, the

551   small differences observed in these spectra are probably due to differences in the orientation

552   of the calcite crystals with respect to the polarised nature of the X-ray beam (see

553   Supplementary Information for more detail). Some of the differences observed between

554   these spectra, however, may be the result of electronic or crystal-structure changes induced

555   by structural incorporation of Sr or Mn into the calcite lattice. The other two Ca XANES

556   spectra from granules recovered from Hamble soil (i.e. 2 of the 45 spectra) are indicative of

557   mainly vaterite and are represented on Fig 5 by the spectrum labelled HS100 Point C. The

558   remaining 4 spectra obtained from granules recovered from YSH (e.g. YSH Point B in Fig. 5)

559   are also indicative of vaterite. The difference in the pre-edge region between the two

560   polymorphs is clearly shown in the difference in the derivative spectra near 4.039 keV shown

561   in the inset of Fig 5.

562   Hence the Ca K-edge XANES analysis only indicates the presence of two calcium

563   carbonate phases. It should be noted that the attenuation length for X-rays just after the Ca

564   K-edge in calcite is around 8 microns, thus each XANES spectrum is from c. 200 μm^3 of the

565   sample. As XAS is an averaging technique, phases that are present at less than about 10

566   volume% will be difficult to identify. We see calcite XANES for nearly all the points sampled

567   in granules obtained from both the Hamble and YSL soils with only an occasional spectrum

568   of vaterite from a Hamble soil granule. Thus, in agreement with the XRD results (Table 4),

569   we conclude calcite is the dominant phase for the HS and YSL granules with vaterite a

570   minority phase in the HS granules. Ca K-edge XANES for granules extracted from YSH

571   indicated the presence of both calcite (YSH Point A, Fig. 5) and vaterite (YSH Point B, Fig.

572   5), with vaterite XANES being recorded more frequently than in the granules from the other

573   soils. Again the Ca K-edge XANES are in broad agreement with the XRD results (Table 4)

574   whereby the mineralogy of the YSH granules is mostly calcite with additional vaterite.

575

576   **3.5.2. Sr K-edge XANES and EXAFS**

577   Sr K-edge XANES spectra recorded from the Sr standards and typical Sr K-edge

578   XANES from the granules are shown in Fig. 6. All the Sr K-edge XANES spectra collected

579   from different granules are presented in the Supplementary Information. The majority of the

580   Sr K-edge XANES spectra resemble the spectra of our standards "Sr adsorbed onto calcite"

581   and "Sr adsorbed onto granule" (Fig. 6), though some small differences are evident in the

582   intensity of the shoulder (or first oscillation) on the high energy side of the white line at c.

583   16.122 keV. As described for such differences observed between the Ca K-edge XANES

584   spectra, these slight variations are probably related to the orientation of the sample with

585   respect to the polarization of the X-ray beam. The Sr K-edge XANES spectra in Fig. 6 for the

586   granules recovered from the soils (except YSH Point B) and the 2 standards for Sr adsorbed

587   onto calcite and granules are very similar to those previously reported in the literature for Sr

588   structurally incorporated into the calcite lattice (Pingatore et al., 1992; Parkman et al., 1998;

589   Fujita et al., 2004; Finch and Allison, 2007). This suggests that during the preparation of our

590   standards "Sr adsorbed onto calcite" and "Sr adsorbed onto granules" Sr has become

591   structurally incorporated into the calcite lattice, either through diffusion or via a dissolution re-

592   precipitation mechanism (Lakshtanov and Stipp, 2007; Stipp and Hochella, 1991; Tang et

593   al., 2008; Tesoriero and Pankow, 1996). Furthermore, it suggests that in the majority of our

594   granules the Sr is structurally bound within the calcite lattice.

595   Some of the Sr K-edge XANES spectra obtained from granules extracted from the

596   YSH soil (i.e. 5 of the 11 spectra) appear to show significant differences to the majority of the

597   Sr K-edge XANES spectra; these spectra are represented in Fig. 6 by spectrum YSH Point

598   B. They are similar both in appearance and also in terms of the energy shift of the white line

599   with respect to the other spectra of Fig. 6 to the Sr K-edge XANES spectrum of the

600   inorganically synthesised Sr co-precipitated vaterite standard. Thus we assign them to Sr

601   structurally incorporated into vaterite, an interpretation supported by the Ca K-edge XANES

602   and XRD results.

603   Of all the Sr K-edge EXAFS spectra from the granules, 34 out of the 35 spectra

604   obtained from 5 different granules produced in the different Sr-amended Hamble soil (e.g.

605   HS100 Points A and B, Fig. 6), all 5 spectra obtained from granules produced in YSL (e.g.

606   YSL Point A, Fig. 6) and 6 of the 11 spectra obtained from granules produced in YSH (e.g.

607   YSH Point A, Fig. 6) look very similar to each other and also to the EXAFS of our standards

608   "Sr adsorbed on calcite" and "Sr adsorbed on granules". These spectra were collected from

609   the same points for which the Sr K-edge XANES spectra were collected, and which

610   suggested that the Sr was structurally bound within the calcite. Pingatore et al. (1992)

611   suggested a model for Sr within the calcite lattice in which the first 3 shells comprise six O

612   atoms, six C atoms and six Ca atoms, respectively. This model, which reflects well the

613   crystal structure reported by Effenberger et al. (1981), also represents the best fit to the Sr

614   K-edge EXAFS spectra for these points whereby Sr is surrounded by six O atoms at a

615   distance of 2.52 Å, followed by a six C atoms and six Ca atoms at a distance of c. 3.33 Å

616   and c. 4.09 Å, respectively (see Table 5).This is the model for incorporation into calcite used

617   by Elzinga and Reeder (2002) in their studies of other elements. It differs from the models

618   used by Parkman et al. (1992) and Finch and Allison (2007), in that they use a shell

619   occupancy of 3 for C in the second coordination shell. However the Sr-C and Sr-Ca

620   distances in our model are similar to those reported in both of those studies.

621   The Sr^{2+} ion is substantially bigger than the Ca^{2+} ion with a six-coordinate ionic radius

622   of 1.21 Å compared with 1.00 Å for Ca (Shannon, 1976) and thus it is expected that the

623   calcite lattice would be locally expanded around a substituting Sr. We find a Sr-O bond

624   distance of c. 2.51 Å compared to 2.36 Å for Ca-O in calcite (Effenberger et al., 1981). The

625   Sr-EXAFS data from granules obtained in HS soils indicates that Sr replaces Ca in the

626   calcite lattice with a local structural distortion of +7.2% for Ca-O bond lengths and +3.4% for

627   Ca-C distances, respectively. For comparison, Finch and Allison (2007), quantified a 6.5%

628   local dilation in the calcite structure as a consequence of the Sr substitution.

629   The Sr substitution into calcite model fits the Sr data at HS100 Point C (Fig. 7); at the

630   same point the Ca K-edge XANES indicated the presence of vaterite (Fig. 5). This apparent

631   discrepancy is due to differences in the sampling volume for Ca and Sr XAS. The

632   attenuation length of X-rays at the Sr K-edge (16.1 keV) in calcium carbonate is c. 350 µm,

633   while just after the Ca K-edge (4.05 keV) it is only 8 µm. Thus the Sr EXAFS will be from the

634   whole granule slice thickness while the Ca XANES represents only the top 8 µm or so.

635   Consequently, while the Ca K-edge XANES data is from vaterite which dominates the outer

636   8 µm of the sample, the Sr K-edge XAS data is from both this vaterite and also from

637   underlying calcite. As the calcite is the dominant phase in the sampled volume the Sr K-edge

638   EXAFS data can be well fitted by the Sr in calcite model. Indeed, the spectrum presented in

639   Fig. 7 has some features that appear to be part way between those of Sr in calcite and those

640   of YSH point B (see below).

641   Although the Sr in calcite model fitted well 6 of the 11 spectra collected from granules

642   produced in YSH, the other 5 spectra resemble YSH Point B in Fig. 7 and these spectra are

643   better fit by another model; (Sr with 8.5 O atoms at 2.55 Å, 5.2 C atoms at 2.95 Å and then

644   3.5 Ca atoms at 4.13 Å; Table 5). This model is the same as that for our standard vaterite

645   co-precipitated with Sr (Table 5). The precise nature of the vaterite crystal structure is still

646   under debate (Demichelis et al., 2012; Kamhi, 1963; Meyer, 1969; Meyer, 1960), but

647   nevertheless it appears that the radial distribution of atoms about the Ca in vaterite is more

648   complex than that of calcite. The "standard" crystallographic model for vaterite (e.g. Kamhi,

649   1963) has Ca-O, Ca-C, Ca-C and Ca-Ca interatomic distances of 2.28 Å, 2.96 Å, 3.32 and

650   4.24 Å, respectively. Ca-XAS results of Becker et al. (2003) on biogenic vaterite showed a

651   vaterite model with distances of 2.37 Å for Ca-O, 3.09 Å for Ca-O or Ca-C and 4.24 Å for Ca-

652   Ca. Due to the disordered nature of the vaterite crystal structure with respect to that of

653   calcite (e.g. Demichelis et al. 2012), authors of Ca-EXAFS studies have been cautious

654   interpreting or fitting shells and quantifying coordination numbers between 2.9 Å and 3.8 Å

655   (Becker et al., 2003; Demichelis et al., 2012; Lam et al., 2007), but it is generally agreed that

656   Ca-O and Ca-Ca distances of 2.37 Å and 4.24 Å, respectively are characteristic of vaterite.

657   Taking into account the size difference between Sr and Ca our Sr K-edge EXAFS results on

658   Sr incorporation into vaterite are in broad agreement with the existing Ca-XAS data on

659   biogenic and inorganically synthesised vaterite (Becker et al., 2003; Lam et al., 2007),

660   strongly suggesting that Sr can substitute for Ca in the vaterite structure. Furthermore, this

661   study provides evidence of this occurring in inorganically synthesized vaterite as well as

662   vaterite biogenically produced by the earthworm *Lumbricus terrestris*.

663

664 **4. CONCLUSIONS**

665   Granules of calcium carbonate secreted by the earthworm *Lumbricus terrestris* in Sr-

666   rich soils, both those amended with Sr in the form of $Sr(NO_3)_2$ and those that are naturally

667   Sr-rich due to mineralisation, are predominantly calcite with minor amounts of vaterite. In

668   contrast to our previous experiments in which granules were produced in Pb-rich soils

669   (Fraser et al., 2011) no aragonite was found; nor did we detect vaterite in our Pb-rich

670   granules. These findings suggest that the chemistry of the soil or soil solution that the

671   earthworms are exposed to influences granule mineralogy. However, we detected no

672   systematic differences in granule mineralogy across the soils investigated in this study

673   despite their significantly different Sr contents.

674   The mode of incorporation of Sr in the granules appears to differ from that of Pb in

675   our previous study. Pb was concentrated around granule edges and was predominantly

676   adsorbed to the granule surface prior to secretion of the granules with smaller amounts

677   present either as Pb in calcite or cerussite. Sr is incorporated throughout the granules giving

678   rise to oscillatory zoning with no Sr-carbonate phase being detected. This reflects the

679   increased incorporation of Sr into the calcite lattice by comparison to that observed for Pb

680   (Fraser et al., 2011).

681   The Sr content of the granules was at the high end of concentrations in calcite

682   previously reported in the literature; distribution coefficients for the partitioning of the Sr into

683   the granules were relatively high compared to those reported for inorganic systems. This

684   may reflect a kinetic effect such as those reported in inorganic systems (e.g. Nehrke et al.,

685   2007; Tang et al., 2008; Tesoriero and Pankow, 1996; Gabitov and Watson, 2006) with the

686   distribution coefficients being lowest for soils in which granule production was also the

687   lowest. The distribution coefficients indicate that, despite their chemical similarities,

688   earthworms are able to metabolically differentiate between Ca and Sr, both in terms of

689   uptake from the soil and incorporation into the calcium carbonate granules which they

690   produce.

691   Whilst granules are unlikely to concentrate Sr from the soil solution relative to Ca, or

692   concentrate Sr from the bulk soil relative to Ca in naturally Sr-rich soils, our results show that

693   if a soil were to experience a significant increase in its Sr concentration, for example by the

694   accidental release of a ^{90}Sr-rich fluid, calcium carbonate granules could accumulate Sr

695   relative to Ca from both the bulk soil and from earthworms. Thus earthworm secreted

696   calcium carbonate granules may have a role to play in the movement of ^{90}Sr in terrestrial

697   ecosystems.

698   Granules have been shown to survive thousands of years in the soil (e.g. Canti,

699   2007), The use of granules as a record of palaeotemperatures is currently being explored

700   (Versteegh et al., 2012). Our findings, that Sr substitutes into the granules with minimal

701   modification of the calcite structure is encouraging for its use as a palaeoproxy. However the

702   use of soil-based mineral palaeoproxies is fraught with difficulty due to the heterogeneity of

703   soils. Much further work on the impact of soil chemistry and temperature on the partitioning

704   of Sr into earthworm secreted calcium carbonate would be required before the full potential

705   of granule trace element chemistry as a palaeoproxy can be assessed.

706

713

REFERENCES

714

715 Achal V.Pan X. and Zhang D. (2012) Bioremeidation of strontium (Sr) contaminated aquifer

716   quartz sand based on carbonate precipitation induced by Sr resistant Halomonas sp.

717   *Chemosphere* **89**, 764-768.

718 Arnold, R. E. and Hodson, M. E. (2007) Effect of time and mode of depuration on tissue

719   copper concentrations of *Eisenia andrei*, *Lumbricus rubellus* and *Lumbricus*

720   *terrestris*. *Environmental Pollution* **148**, 21–30.

721 Barker S. L. L. and Cox S. F. (2011) Oscillatory zoning and trace element incorporation in

722   hydrothermal minerals: insights from calcite growth experiments. *Geofluids* **11**, 48-

723   56.

724 Barouki T.H., Martinez B.C., Mortensen B.M., Weathers T.S., DeJong J.D. Ginn T.R.,

725   Spycher N.F., Smith R.W. and Fujita Y. (2011) Forward and inverse bio-geochemical

726   modelling of microbially induced calcite precipitation in half-meter column

727   experiments. *Transport in porous media* **90** Special Issue, 23-39

728 Becker A., Bismayer U., Epple M., Fabritius H., Hasse B., Shi J. and Ziegler A. (2003)

729   Structural characterisation of X-ray amorphous calcium carbonate (ACC) in sternal

730   deposits of the crustacea Porcellio scaber. *Dalton Transactions* 551-555.

731 Bentov, S. and Erez, J. (2006) Impact of biomineralization processes on the Mg content of

732   foraminiferal shells: A biological perspective. *Geochemistry, Geophysics,*

733   *Geosystems*, **7**, doi:10.1029/2005GC001015.

734 Berner, R.A. (1975) The role of magnesium in the crystal growth of calcite and aragonite

735   from sea water. *Geochemica et Cosmochimica Acta*, **39**, 489-504.

736 Bluszcz P., Lucke A., Ohlendorf C. and Zolitchka B. (2009) Seasonal dynamics of stable

737   isotopes and element ratios in authigenic calcites during their precipitation and

738   dissolution, Sacrower See (northeastern Germany). *Journal of Limnology* **68** 257-

739   273.

740 Bots P. (2012) Experimental investigations of calcium carbonate mineralogy in past and

741   present oceans. Unpublished PhD Thesis, The University of Leeds.

742 Bots P., Benning L. G., Rickaby R. E. M. and Shaw S. (2011) The role of SO_4 in the switch

743   from calcite to aragonite seas. *Geology* **39**, 331-334.

744 Bracco J.N., Grantham M.C. and Stack A.G. (2012) Calcite growth rates as a function of

745   aqueous calcium-to-carbonate ratio, saturation index, and inhibitor concentration:

746   Insight into the mechanism of reaction and poisoning by strontium. *Crystal Growth*

747   *and Design* **12**, 3540-3548.

748 Briones M. J. I., Ostle N. J. and Piearce T. G. (2008) Stable isotopes reveal that the

749   calciferous gland of earthworms is a CO_2-fixing organ. *Soil Biology and Biochemistry*

750   **40**, 554-557.

751 BSI (2005) ISO 10390:2005 Soil quality. Determination of pH. British Standards Online.

752 BSI (2009) BS EN 15935. Soil, sludge, waste, and treated biowaste. Determination of loss

753   on ignition. British Standards Online.

754 BSI (2010) ISO 12914. Soil quality. Microwave-assisted extraction of the aqua regia soluble

755   fraction for the determination of elements. British Standards Online.

756 Canti M. G. and Piearce T. G. (2003) Morphology and dynamics of calcium carbonate

757   granules produced by different earthworm species: *The 7th international symposium*

758   *on earthworm ecology, Cardiff, Wales, 2002. Pedobiologia* **47**, 511-521.

759 Canti M. G. (2009) Experiments on the origin of ^{13}C in the calcium carbonate granules

760   produced by the earthworm *Lumbricus terrestris*. *Soil Biology and Biochemistry* **41**,

761   2588-2592.

762 Canti M.G. (2007) Deposition and taphonomy of earthworm granules in relation to their

763   interpretative potential in Quaternary stratigraphy. *J. Quatern. Sci.* **22**, 111-118.

764 Chwodhury M. J., van-Ginneken L. and Blust R. (2000) Kinetics of waterborne strontium

765   uptake in the common carp., Cyprinus carpio, at different calcium levels.

766   *Environmental Toxicological and Chemistry* **19**, 622-630.

767   Darwin C. R. 1881.*The formation of vegetable mould, through the action of worms, with*

768   *observations on their habits.* John Murray, London

769   Demichelis R., Raiteri P., Gale J. D. and Dovesi R. (2012) A new structural model for

770   disorder in vaterite from first-principles calculations. *CrystEngComm* **14**, 44-47.

771   DePaolo D.J. (2012) Surface kinetic model for isotopic and trace element fractionationduring

772   precipitation of calcite from aqueous solutions. *Geochimica et Cosmochimica Acta*

773   **75**, 1039-1056.

774   Dissard D., Nehrke G., Reichart G and Bijma J. (2010a) The impact of salinity on the Mg/Ca

775   and Sr/Ca ratio in the benthic foraminifera *Ammonia tepida*: Results from culture

776   experiments. *Geochimica et Cosmochimica Acta* **74** 928-940.

777   Dissard D., Nehrke G., Reichart G and Bijma J. (2010b) Impact of seawater pCO2 on

778   calcification and Mg/Ca and Sr/Ca ratios in benthic foraminifera calcite: results from

779   culturing experiments with *Ammonia tepida*. *Biogeosciences* **7**, 81-93.

780   Dodd J. (1967) Magnesium and strontium in calcareous skeletons: A review. *Journal of*

781   *Palaeontology* **41**, 131-1329.

782   Edwards C. A. (2004) Earthworm Ecology. CRC Press, Boca Raton, Florida.

783   Edwards C. A. and Bohlen P. J. (1996) *Biology and Ecology of Earthworms*. Chapman &

784   Hall, London.

785   Effenberger H., Mereiter K. and Zemann J. (1981) Crystal structure refinements of

786   magnesite, calcite, rhodochrosite, siderite, smithonite, and dolomite, with discussion

787   of some aspects of the stereochemistry of calcite type carbonates. *Zeitschrift fur*

788   *Kristallographie* **156**, 233-243.

789   Elzinga E. J. and Reeder R. J. (2002) X-ray absorption spectroscopy study of Cu^{2+} and Zn^{2+}

790   adsorption complexes at the calcite surface: Implications for site-specific metal

791   incorporation preferences during calcite crystal growth. *Geochimica et Cosmochimica*

792   *Acta* **66**, 3943-3954.

793   Fairchild I.J., Borsato A., Tooth A.F., Frisia S., Hawkesworth C.J., Huang Y., McDermott F.

794   and Spiro B. (2000). Controls on trace element (Sr–Mg) compositions of carbonate

795   cave waters: implications for speleothem climatic records. *Chemical Geology* **166**,

796   255–269.

797   Fernández-Díaz, L., Putnis, A., Prieto, M. and Putnis, C. (1996) The role of magnesium in

798   the crystallization of calcite abd aragonite in a porous medium. *Journal of*

799   *Sedimentary Research*, **66**, 482-491.

800   Finch A. A. and Allison N. (2007) Coordination of Sr and Mg in calcite and aragonite.

801   *Mineralogical Magazine* **71**, 539-552.

802   Fraser A., Lambkin D. C., Lee M. R., Schofield P. F., Mosselmans J. F. W. and Hodson M.

803   E. (2011) Incorporation of lead into calcium carbonate granules secreted by

804   earthworms living in lead contaminated soils. *Geochimica et Cosmochimica Acta* **75**,

805   2544-2556.

806   Fujita Y., Taylor J.L., Wendt L.M., Reed D.W. and Smith R.W. (2010) Evaluating the

807   potential of native ureolytic microbes to remediate a Sr-90 contaminated

808   environment. *Environmental Science and Technology* **44** 7652-7658.

809   Fujita Y., Redden G. D., Ingram J. C., Cortez M. M., Ferris F. G. and Smith R. W. (2004)

810   Strontium incorporation into calcite generated by bacterial ureolysis. *Geochimica et*

811   *Cosmochimica Acta* **68**, 3261-3270.

812   Gabitov R. I. and Watson E. B. (2006) Partitioning of strontium between calcite and fluid.

813   *Geochemistry, Geophysics, Geosystems* **7**,12.

814   Gago-Duport L., Briones M., Rodríguez J. and Covelo B. (2008) Amorphous calcium

815   carbonate biomineralization in the earthworm's calciferous gland: pathways to the

816   formation of crystalline phases. *Journal of Structural Biology* **162**, 422-35.

817   Gebauer D., Gunawidjaja P. N., Ko J. Y. P., Bacsik Z., Aziz B., Liu L., Hu Y., Bergström P.

818   L., Tai C.-W., Sham T.-K., Edén D. M. and Hedin N. (2010) Proto-Calcite and Proto-

819   Vaterite in Amorphous Calcium Carbonates. *Angewandte Chemie International*

820   *Edition* **49**, 8889-8891.

821   Gray J., Jones S. R. and Smith A. D. (1995) Discharges to the environment from the

822   Sellafield site, 1951-1992. *Journal of Radiological Protection* **15**, 99-131.

823 Gruzensky P. M. (1967) Growth of calcite crystals. In: Peiser, H. S. (Ed.),*Crystal Growth*.

824   Pergamon, Oxford.

825 Gu B. H., Wu W. M., Ginder-Vogel M. A., Yan, H., Fields M. W., Zhou J., Fendorf S., Criddle,

826   C.S. and Jardine P.M. (2005). Bioreduction of uranium in a contaminated soil

827   column. *Environmental Science and Technology* **39**, 4841-4847.

828 Hayakawa S., Hajima Y., Qiao S., Namatame H. and Hirokawa T. (2008) Characterization of

829   Calcium Carbonate Polymorphs with Ca K Edge X-ray Absorption Fine Structure

830   Spectroscopy. *Analytical Sciences* **24**, 835-837.

831 ISO (1993) ISO 11465:1993, Soil quality *Determination of dry matter and water content on a*

832   *mass base - Gravimetric method*, ISO.

833 Kamhi S. (1963) On the structure of vaterite $CaCO_3$. *Acta Crystallographica* **16**, 770-772.

834 Lakshtanov L. Z. and Stipp S. L. S. (2007) Experimental study of nickel(II) interaction with

835   calcite: Adsorption and coprecipitation. *Geochimica et Cosmochimica Acta* **71**, 3686-

836   3697.

837 Lam R. S. K., Charnock J. M., Lennie A. and Meldrum F. C. (2007) Synthesis-dependant

838   structural variations in amorphous calcium carbonate. *CrystEngComm* **9**, 1226-1236.

839 Lambiv-Dzemua G., Gleeson S. A. and Schofield P. F. (2012) The importance of lithiophorite

840   over asbolane in the ore zone mineralogy of the Nkamouna Co-Mn laterite deposit,

841   southeast Cameroon. *Mineralium Deposita* submitted.

842 Lambkin D. C., Gwilliam K. H., Layton C., Canti M. G., Piearce T. G. and Hodson M. E.

843   (2011) Production and dissolution rates of earthworm-secreted calcium carbonate.

844   *Pedobiologia,* **54**, S119-S129.

845 Lee M. R., Hodson M. E. and Langworthy G. (2008) Earthworms produce granules of

846   intricately zoned calcite. *Geology* **36**, 943-946.

847 Lorens, R.B. and Bender, M.L (1977) Physiological exclusion of magnesium from *Mytilus*

848   *edulis* calcite. *Nature*, **269**, 793-794.

849 Loste, E., Wilson, R.M., Seshadri, R. and Meldrum, F.C. (2003) the role of magnesium in

850 stabilising amorphous calcium carbonate and controlling calcite morphologies.

851 *Journal of Crystal Growth*, **254**, 206-218.

852 Meyer H. (1960) Ueber Vaterit und seine Struktur. *Fortschritte der Mineralogie* **38**, 186-187.

853 Meyer H. (1969) Struktur und fehlordnung des vaterits. *Zeitschrift fuer Kristallographie,*

854 *Kristallgeometrie, Kristallphysik, Kristallchemie (-144,1977)* **128**, 183-212.

855 Morgan A.J. (1981) A morphological and electron-microprobe study of the inorganic

856 composition of the mineralized secretory products of the calciferous gland and

857 chloragogenous tissue of the earthworm, *Lumbricus terrestris* L. The distribution of

858 injected strontium. *Cell and Tissue Research* **220**, 829-844.

859 Morgan J. E., Richards S. P. G. and Morgan A. J. (2001) Stable strontium accumulation by

860 earthworms: a paradigm for radiostrontium interactions with its cationic analogue,

861 calcium. *Environmental Toxicology and Chemistry* **20**, 1236-1243.

862 Morgan J. E., Richards S. P. G. and Morgan A. J. (2002) Contrasting accumulative patterns

863 of two cationic analogues, Ca and Sr, in ecophysiologically contrasting earthworm

864 species (*Aporrectodea longa* and *Allolobophora chlorotica*) from the field. *Applied*

865 *Soil Ecology* **21**, 11-22.

866 Morse, J.W., Wang, Q.W. and Tsio, M.Y. (1997) Influences of temperature and Mg:Ca ratio

867 on $CaCO_3$ preciptiates from seawater. *Geology* **25**, 85-87.

868 Mosselmans J. F. W., Quinn P. D., Dent A. J., Cavill S. A., Diaz-Moreno S., Peach, A.,

869 Leicester P. J., Keylock S. J., Gregory S., Atkinson K. D. and Roque Rosell J. (2009)

870 I18-the microfocus spectroscopy beamline at the Diamond Light Source. *Journal of*

871 *Synchrotron Radiation* **16**, 818-824.

872 Nahmani J., Hodson M. E. and Black, S. (2007) A review of studies performed to

873 assessmetal uptake by earthworms. *Environmental Pollution* **145**, 402-424.

874 Nehrke G., Reichart G., van-Capellen P., Meile C. and Bijma J. (2007) Dependence of

875 calcite growth rate and Sr partitioning on solution stoichiometry: Non-Kossel crystal

876 growth. *Geochimica et Cosmochimica Acta* **71**, 2240 - 2249.

877   Nickless E., Booth S. and Mosley P. (1976) The celestite resources of the north-east of

878   Bristol with notes on occurrences north and south of the Mendip Hills and in the Vale

879   of Glamorgan: Description of the 1:25000 resource sheet ST68 and parts of ST59,

880   69, 79, 58, 78, 67 and 77. In: Sciences, I. o. G. (Ed.), Edinburgh, UK.

881   Parkman R. H., Charnock J. M., Livens F. R. and Vaughan, D. J. (1998) A study of the

882   interaction of strontium ions in aqueous solution with the surfaces of calcite and

883   kaolinite. *Geochimica et Cosmochimica Acta* **62**, 1481-1492.

884   Perdrial N., Rivera N., Thompson A., O'Day P.A. and Chorover J. (2011) Trace contaminant

885   concentration ffects mineral transformation and pollutant fate in hydroxide-weathered

886   Hanford sediments. *Journal of Hazardous Waste* **197**, 119-127.

887   Piearce T.G. (1972) The calcium relations of selected *Lumbricidae*. *Journal of Animal*

888   *Ecology* **41**,167–188.

889   Pingitore Jr. N. E., Lytle F. W., Davies B. M., Eastman M. P., Eller, P. G. and Larson E. M.

890   (1992) Mode of incorporation of Sr^{2+} in calcite: Determination by X-ray absorption

891   spectroscopy. *Geochimica et Cosmochimica Acta* **56**, 1531-1538.

892   Radha, A.V, Fernandez-Martinez, A., Hu, Y., Young-Shin, J, Waychunas, G.A. and

893   Navrotsky, A. (2012) Energetic and structural studies of amorphous Ca_{1-}

894          $_xMg_xCO_3.nH_2O$ ($0 \leq x \leq 1$). *Geochimica et Cosmochimica Acta* **90**, 83-95.

895   Ravel B. and Newville M. A. (2005) ATHENA, ARTEMIS, HEPHAESTUS: data analysis for

896   X-ray absorption spectroscopy using IFEFFIT. *Journal of Synchrotron Radiation* **12**,

897   537-541.

898   Raz, S., Weiner, S. and Addadi, L/ (2000) Formation of high-magnesian calcites via an

899   amorphous precursor phase: Possible biological implications. *Advanced materials*

900   **12**, 38-42.

901   Reis, J.B., Anderson, M.A. and Hill, R.T. (2008) Seawater Mg/Ca controls polymorph

902   mineralogy of microbial $CaCO_3$: A potential proxy for calcite-aragonite seas in

903   Precambrian time. *Geobiology* **6**, 106-119.

904 Riley R.G.; Zachara J.M. and Wobber F.J. (1992) Chemical contamiannts on DOE Lands

905   and selection of contaminant mixture for subsurface science research. DOE/ER-

906   0547T; U.S. Department of Energy, Office of Energy Research: Washington, DC,

907 Robertson J. D. (1963) The Function of the Calciferous Glands of Earthworms. *Journal of*

908   *Experimental Biology* **13**, 279-297.

909 Rodriguez-Blanco J. D., Bots P., Rocal-Herrero T., Shaw S. and Benning L. G. (2011a) The

910   role of Mg in the formation of monohydrocalcite *Mineralogical Magazine* **75**, 1741.

911 Rodriguez-Blanco J. D., Shaw S. and Benning L. G. (2011b) The kinetics and mechanisms

912   of amorphous calcium carbonate (ACC) crystallization to calcite, via vaterite.

913   *Nanoscale* **3**, 265-271.

914 Schofield P. F., Knight K. S., Covey-Crump S. J., Cressey G. and Stretton I. C. (2002)

915   Accurate quantification of the modal mineralogy of rocks when image analysis is

916   difficult. *Mineralogical Magazine* **66**, 189–200.

917 Shannon R. D. (1976) Revised effective ionic radii and systematic studies of interatomic

918   distances in halides and chalcogenides. *Acta Crystallographica* **A32**, 751-767.

919 Shore M. and Fowler A. D. (1996) Oscillatory zoning in minerals; a common phenomenon.

920   *The Canadian Mineralolgist* **34**, 1111-1126.

921 Sinclair D.J., Banner J.L., Taylor F.W., Partin J., Jenson J., Mylroie J. Goddard E. Quinn T.,

922   Jocson J. and Miklavic B. (2012) Magnesium and strontium systematics in tropical

923   speleothems from the Western Pacific. *Chemical Geology* **294**, 1-17.

924 Solé V. A., Papillon E., Cotte M., Walter P. and Susini J. (2007) A multiplatform code for the

925   analysis of energy-dispersive X-ray fluorescence spectra. *Spectrochimica Acta* **62**,

926   63-68.

927 Spycher N., Weathers T., Barkouki T., Smith R.W., Ginn T.R., Zhang G.X. Fujita Y., Wu

928   Y.X., Ajo-Franklin J., hubbard S. and Sengor S.S. (2009) Remediation of Sr-90 by

929   induced calcite precipitation: Reactive transport modelling on several fronts. *Abtracts*

930   *of paper of the American Chemical Society* **237,** Abstract 114-GEOC

931   Standring W.J.F., Oughton D.H. and Salbu B. (2002) Potential remobilisation of Cs-137, Co-

932   60, Tc-99 and Sr-90 from contaminated Mayak sediments river and estuary

933   environments. *Environmental Science and Technology* **36**, 2330-2337.

934   Stipp S. L. and Hochella M. F. (1991) Structure and bonding environments at the calcite

935   surface as observed with X-ray photoelectron spectroscopy (XPS) and low energy

936   electron diffraction (LEED). *Geochimica et Cosmochimica Acta* **55**, 1723-1736.

937   Stoll H.M., Klaas C.M., Probert I., Encinar J.R. and Alonso J.I.G. (2002) Calcification rate

938   and temperature effects on Sr partitioning in coccoliths of multiple species of

939   coccolithophorids in culture. *Global and Planetary Change* **34**, 153_171

940   Tang J., Köhler S. J. and Dietzel M. (2008) Sr^{2+}/Ca^{2+} and $^{44}Ca/^{40}Ca$ fractionation during

941   inorganic calcite formation: I. Sr incorporation. *Geochimica et Cosmochimica Acta*

942   **72**, 3718-3732.

943   Tenderholt A. and Quinn P. (2009) PySpline. Free Software Foundation, Inc., Boston, USA.

944   Tertre E., Page J. and Beaucaire C. (2012) Ion exchange model for reversible sorption of

945   divalent metals on calcite: Implications for natural environments. *Environmental*

946   *Science and Technology* **46**, 10055-10062.

947   Tesoriero A. J. and Pankow J. F. (1996) Solid solution partitioning of Sr^{2+}, Ba^{2+}, and Cd^{2+} to

948   calcite. *Geochimica et Cosmochimica Acta* **60**, 1053-1063.

949   Thompson A., Steefel C.I., Perdrial N. and Chorover J. (2010) Contaminant desoprtion

950   during long-term leaching of hydroxide-weathered Hanford sediments. *Environmental*

951   *Science and Technology* **44**, 1992-1997.

952   Tomic S., Searle B. G., Wander A., Harrison N. M., Dent A., Mosselmans J. F. W. and

953   Inglesfield J. E. (2004) DL-EXCURV. STFC Daresbury Laboratory, Daresbury, UK.

954   Veizer J. (1983) Trace elements and isotopes in sedimentary carbonates. *Carbonates*

955   *Mineralogy and Chemistry; Reviews in Mineralogy* **11**, 265–299.

956   Versteegh E.A.A., Hodson M.E. and Black S. (2012) Earthworm secreted calcium carbonate

957   – a new palaeothermometer? 22nd Goldschmidt Conference, Montreal, Canada.

958   Abstract volume.

959   Wang, D., Hamm, L.M., GIuffre, A.J., Echigo, T., Rimstidt, J.D., de Yoreo, J.J., Grotzinger, J.

960   and Dove, P.M. (2012) Revisiting geochemical controls on patterns of carbonate

961   depostion through the lens of multiple pathways to mineralisation. *Faraday*

962   *Discussions* **159**, 371-386.

963   Warren L. A., Maurice P. A., Parmar N. and Ferris F. G. (2001) Microbially Mediated Calcium

964   Carbonate Precipitation: Implications for Interpreting Calcite Precipitation and for

965   Solid-Phase Capture of Inorganic Contaminants. *Geomicrobiology Journal* **18**, 93-

966   115.

967   Wassenburg J.A., Immenhauser A., Richter D.K., Jochum K.P., Fietzke J., Deininger M.,

968   Goos M., Scholz D., Sabaoui A. (2012) Climate and cave control on

969   Pleistocene/Holocene calcite-to-aragonite transitions in speleothems from Morocco:

970   Elemental and isotopic evidence. *Geochimica et Cosmochimica Acta* 92, 23-47.

971

972 **Figure Captions**
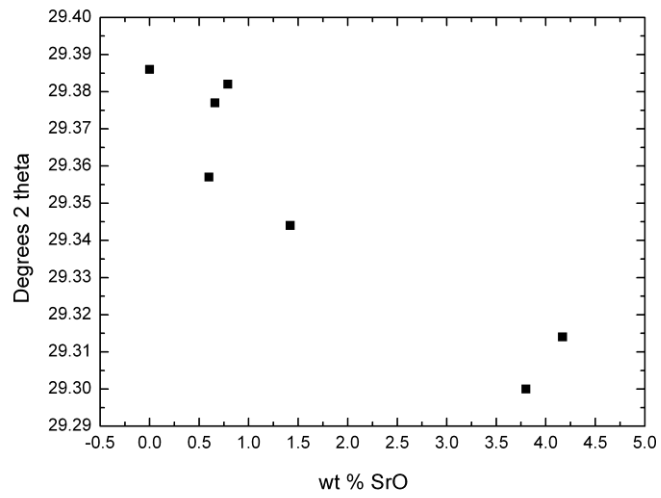
973
974 **Figure 1.** Plot of the calcite 104 peak position (λ = Cu Kα_1) as a function of average wt%

975 SrO as estimated from point EPMA analyses across a core-rim line profile.

976
977

978   **Figure 2.** Optical images of granules produced by *L. terrestris* in Hamble soils amended with

979   various Sr concentrations showing the two general morphological types that the granules
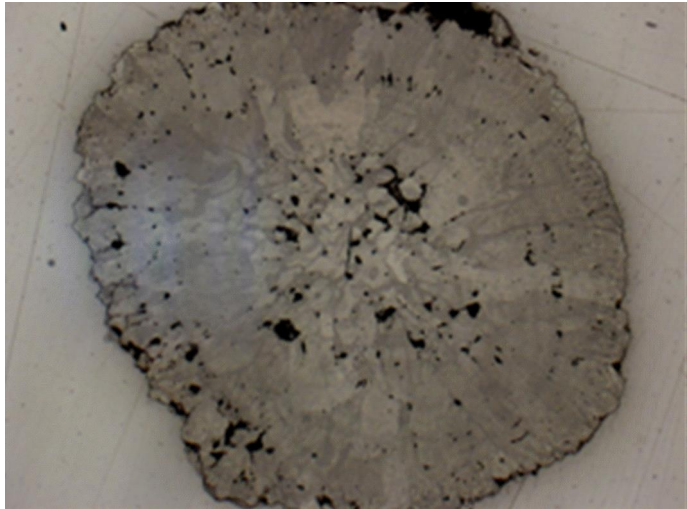
980   displayed. (a) is a granule from HS500

981   (b) is a granule from HS100. Granules are c. 2 mm in diameter.

982

983

984

985

986   **Figure 3.** Sr distribution maps from EPMA of granules produced by *L. terrestris* in Hamble

987   soils amended with various Sr concentrations.

988   (a) a granule recovered from the depurate of earthworms kept in HS100
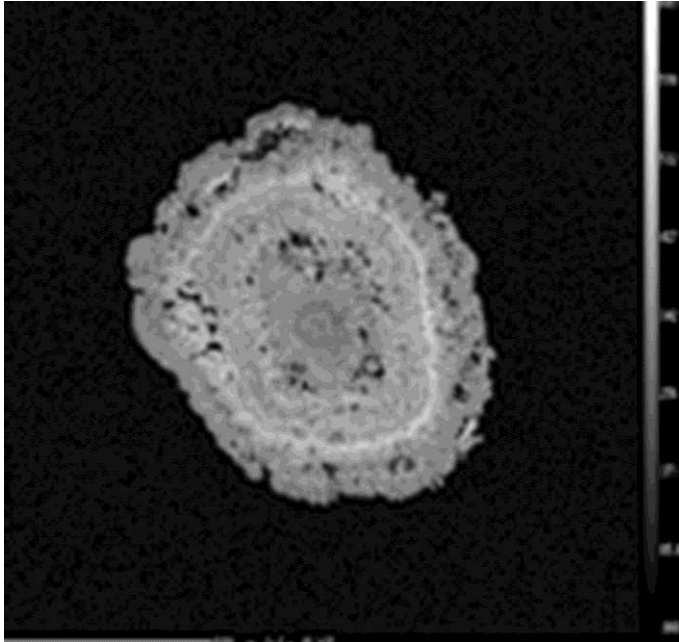
989
990

991   (b) a granule recovered from the depurate of earthworms kept in HS100
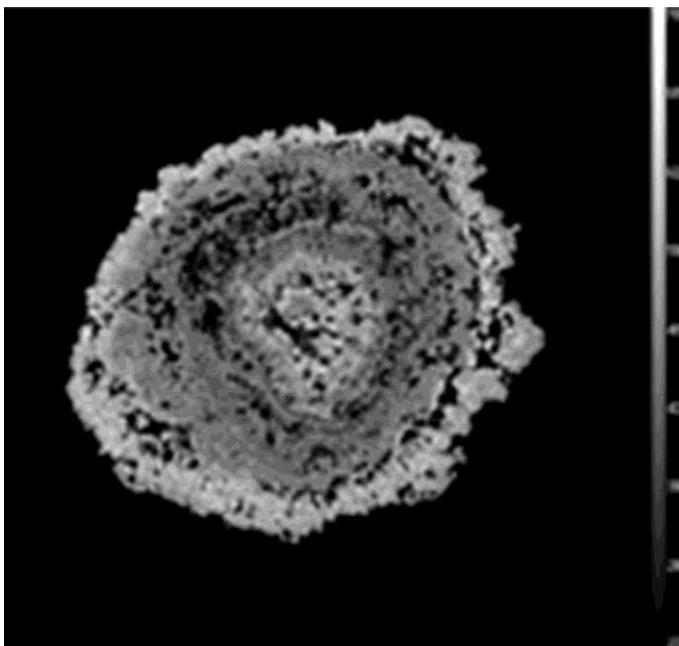

992
993
994

40
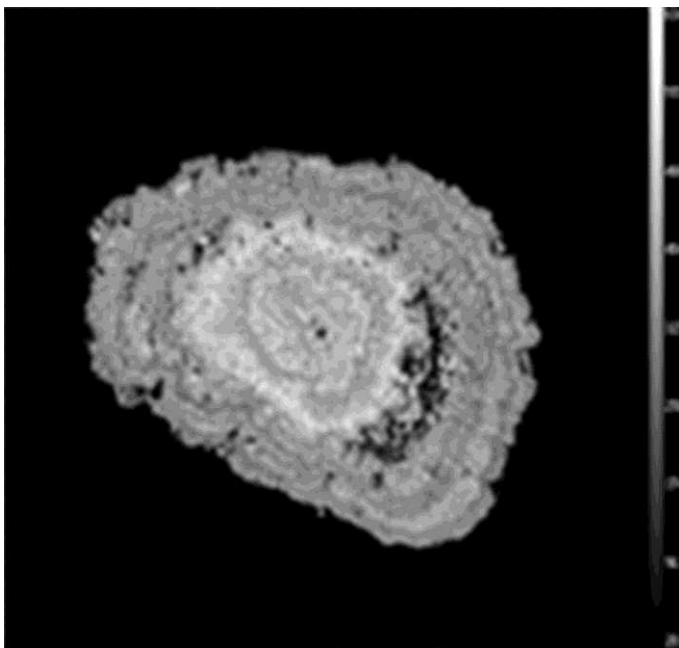
995 (c) a granule extracted from HS500 and
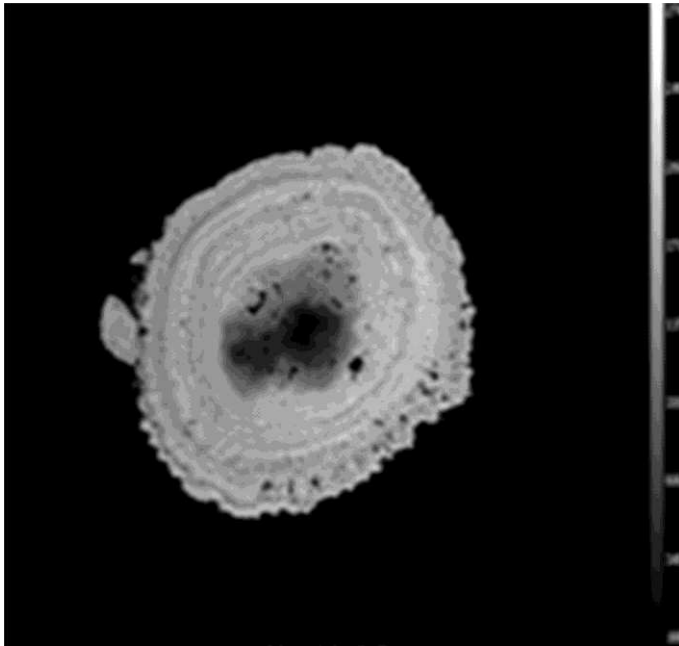
996

997

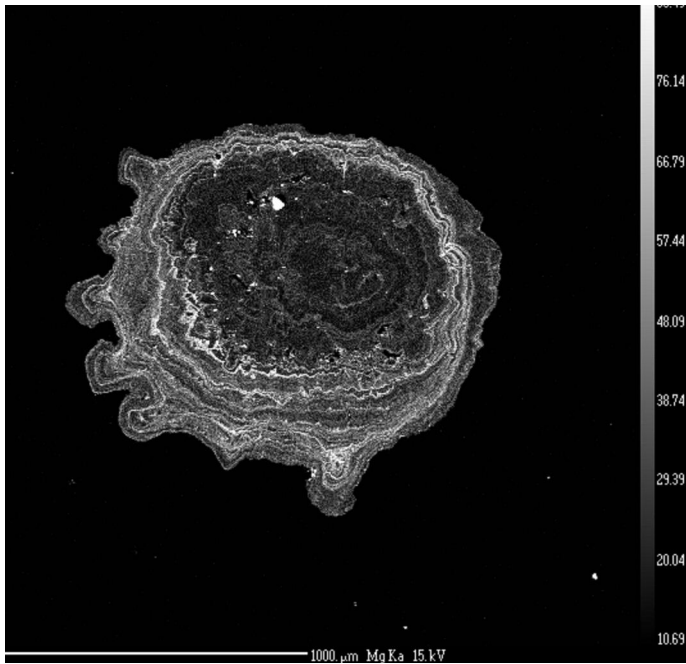998 (d) a granule extracted from HS100.

999

1000

1001   **Figure 4.** Mg and Mn distribution maps from EPMA of granules produced by *L. terrestris* in

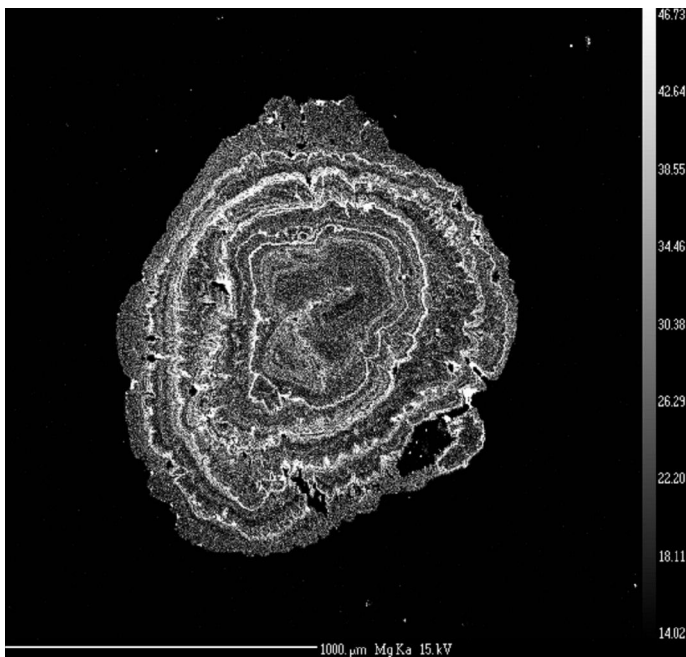1002   Hamble soils amended with various Sr concentrations.

1003   (a) Mg map from a granule from HS150

1004

1005

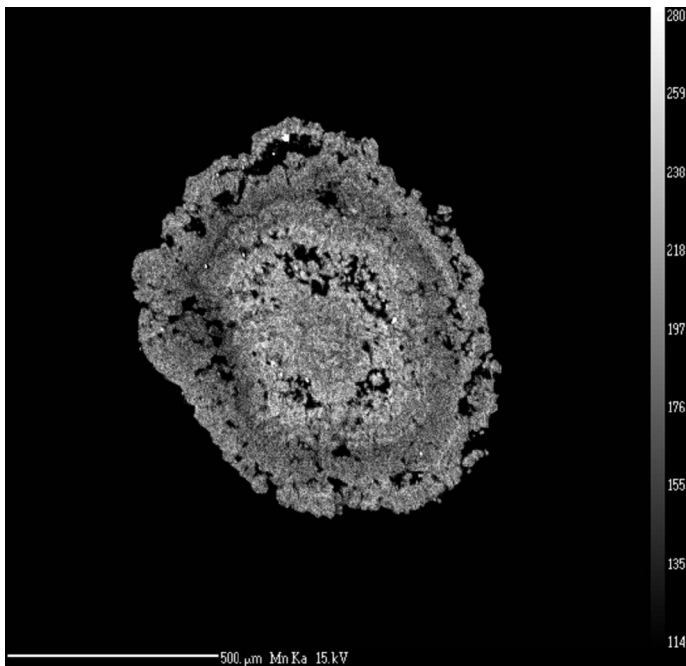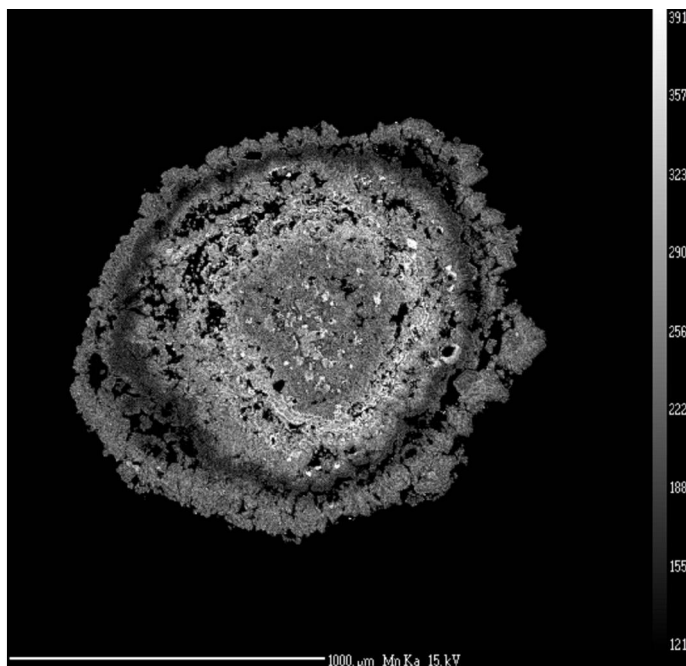1006   (b) Mg map of a granule from HS100

1007

1008

1009

1010   (c) Mn map of a granule recovered from the depurate of an earthworm kept in HS100 and


1011

1012

1013   (d) Mn map of a granule from HS100.

1014

1015 **Figure 5.** Ca K-edge XANES spectra for the carbonate standards: calcite (data from Fraser

1016 et al., 2011), Sr-bearing aragonite (obtained from Dr A. Finch, University of St Andrews) and

1017 synthetic vaterite (obtained from Dr P. Bots, University of Leeds) andfor selected points from

1018 individual granules extracted from HS100, YSL and YSH. The first derivative of the pre-edge

1019 and edge are shown in the inset. . "1", "2", "3" and "4" highlight diagnostic features of the

1020 spectra (see text for details).

1021
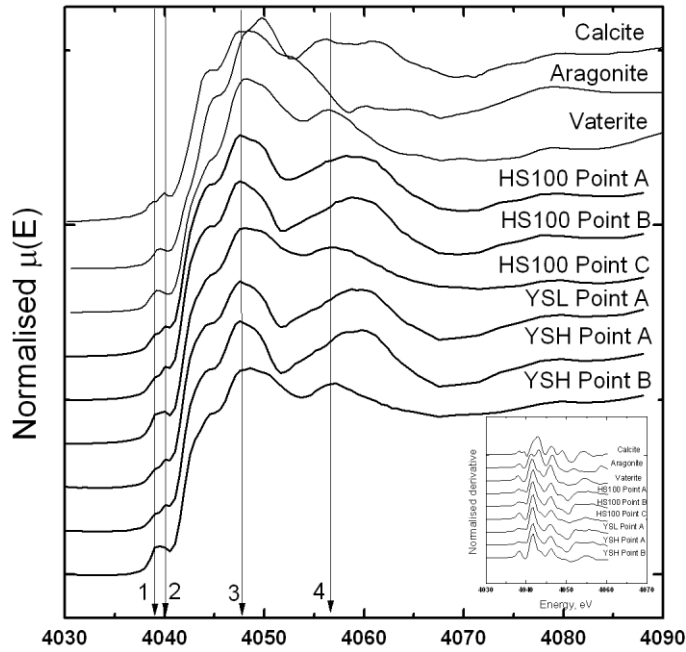
1022

1023   **Figure 6.** Sr K -edge XANES spectra for the Sr standards used in this study and for three

1024   points on a granule from HS100 (HS100 Points A to C), a point on a granule from YSL (YSL

1025   Point A) and two points on a granule from YSH (YSH Point A and B). Spectra were collected

1026   from the same points as those in Fig. 5. For the standards "Sr ads onto calcite" and "Sr ads

1027   onto granule" are for Sr adsorbed onto calcite and granules, respectively. "Vaterite copp with

1028   Sr" is for the synthetic vaterite co-precipitated with Sr.
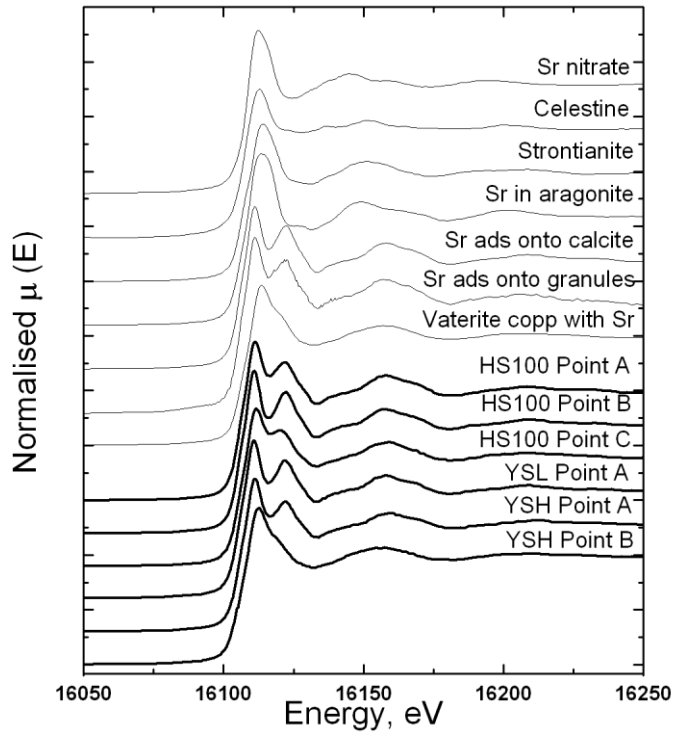
1029

1030

1031 **Figure 7.** k^3-weighted EXAFS spectra with EXAFS model (dotted line) for the same data as
1032 Fig. 6.
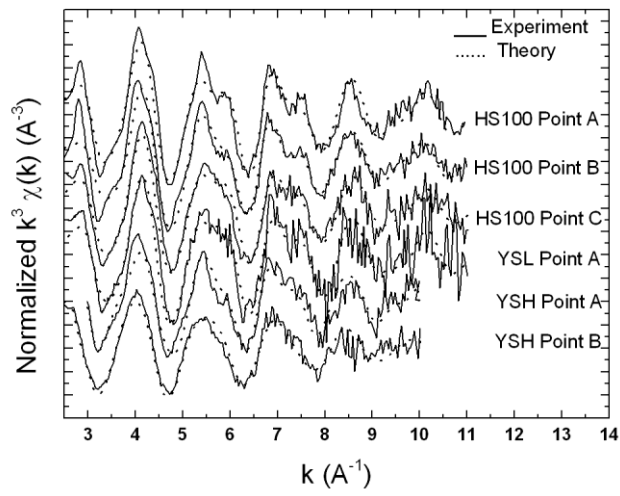
1033
1034

Table 1. Soil properties. Values are mean ± s.d. with number of replicates given in brackets.

Parameter /Soil	HS	HS50	HS100	HS150	HS500	YSL	YSH
pH	8.3	8.18 ± 0.10	8.24 ± 0.02	8.24 ± 0.0	8.05 ± 0.06	5.62 ± 0.16	8.06 ± 0.22
	(n = 1)	(n = 5)	(n = 5)	(n = 5)	(n = 5)	(n = 5)	(n = 5)
WHC / % (n = 3)	39.9 ± 0.5	ND[a]	ND[a]	ND[a]	ND[a]	74.9 ± 0.2	51.4 ± 9.4
Organic matter content (LOI) / %	3.0	ND[a]	ND[a]	ND[a]	ND[a]	9.2	3.2
(n = 1)							
Target Sr concentration / mg kg^{-1}	-	50	100	150	500	-	-
Actual Soil Sr / mg kg^{-1}	32 ± 2	72 ±6	145 ± 42	180 ± 30	600 ± 50	950 ± 50	11000 ± 900
	(n = 3)	(n = 5)	(n=5)	(n=5)	(n=5)	(n=5)	(n=5)
Soil Ca / mg kg^{-1}	8550 ± 990	8 600 ± 400	8 900 ± 500	8 100 ± 400	9 800 ± 300 (n =	3 540 ± 240	24 100 ± 800
	(n = 3)	(n = 5)	(n = 5)	(n = 5)	5)	(n = 5)	(n = 5)
Soil solution Sr / mg L^{-1}	ND[a]	5.58 ± 1.35	10.1 ± 2.79	19.7 ± 1.96	131 ± 25.28	21.9 ± 10.9	80.8 ± 11.6
		(n = 5)	(n = 5)	(n = 5)	(n = 5)	(n = 5)	(n = 5)
Soil solution Ca / mg L^{-1}	ND[a]	288 ± 81	298 ± 55	359 ± 117	790 ± 49	95 ± 44	228 ± 38

[a]ND = Not determined, property assumed to be unaffected by addition of Sr salt to Hamble soil

Table 2. Earthworm and granule data. Values either represent mean values $\pm$ s.d. (n = 5) or, for granules, single values derived from the combining of all 5 replicates to give sufficient mass for accurate measurement and analysis.

Parameter /Soil	HS	HS50	HS100	HS150	HS500	YSL	YSH
Earthworm Sr / mg kg^{-1}	13.6 $\pm$ 6.10	69.1 $\pm$ 17.1	179 $\pm$ 83.5	213 $\pm$ 36.5	708 $\pm$ 112	603 $\pm$ 92.9	4100 $\pm$ 1070
Earthworm Ca / mg kg^{-1}	10600 $\pm$ 1500	10500 $\pm$ 1980	11900 $\pm$ 4300	9550 $\pm$ 1960	11300 $\pm$ 1600	6100 $\pm$ 508	11300 $\pm$ 1500
Granule Sr / mg kg^{-1}	345 $\pm$ 23[a]	4000	7930	12000	34200	14700	51400
Granule Ca mg kg^{-1}	ND	425000	449000	427000	447000	338000	402000
Production rate / mg $CaCO_3$ g$_{worm}$$^{-1}$ day^{-1}	0.28	0.47	0.38	0.32	0.48	0.05	0.19
Production rate / mg $CaCO_3$ earthworm^{-1} day^{-1}	1.52	0.89	1.50	1.67	2.30	0.26	0.74

[a]values taken from Hamble soil data, Lee et al. (2008)

Table 3. Distribution coefficients for Sr and Ca partitioning. Values for soil and soil solution distribution coefficients are mean values $\pm$ s.d. (n = 5). For granules, single values based on the mean soil, soil solution and earthworm concentrations of Sr and Ca and the Sr and Ca concentrations in the pooled granules from all 5 replicates are given.

Components / Soil	HS	HS50	HS100	HS150	HS500	YSL	YSH
Earthworm / soil	0.58 ± 0.22	0.79 ± 0.10	1.01 ± 0.43	1.05 ± 0.29	1.04 ± 0.19	0.37 ± 0.05	0.78 ± 0.09
Earthworm / soil solution	ND	0.36 ± 0.06	0.42 ± 0.19	0.41 ± 0.06	0.38 ± 0.06	0.44 ± 0.05	1.01 ± 0.16
Granule / soil	ND	1.12	1.09	1.27	1.25	0.16	0.28
Granule / soil solution	ND	0.50	0.50	0.51	0.46	0.19	0.36
Granule / earthworm	ND	1.43	1.17	1.26	1.22	0.44	0.35

49

Table 4. The calcium carbonate mineralogy as identified by XRD (XRD-NHM and μXRD-NHM) and the trace element chemistry from EPMA of granules. The calcite 104 peak 2θ position is provided based upon the wavelength of Cu Kα$_1$ radiation. The average wt% SrO, MgO and MnO levels are taken from EPMA analyses within a rim-to-core line profile.

Sample name	Carbonate phases identified	Calcite 104 peak 2θ (XRD-NHM)	Range of SrO concentrations	Average wt % SrO	Range of MgO concentrations	Average wt % MgO	Range of MnO concentrations	Average wt % MnO
HS control	calcite, vaterite	29.386(2)	0	0.04[a]	-	0.06[a]	-	0.02[a]
HS50	calcite, vaterite	29.357(2)	0.48-0.83	0.60	0.04-0.017	0.08	0.20-0.39	0.30
HS100	calcite, vaterite	29.377(2)	0.10-1.58	0.66	0.06-0.23	0.12	0.05-0.55	0.22
HS100 FRESH[b]	Calcite	29.382(2)	0.56-1.14	0.79	0.02-0.17	0.07	0.19-0.41	0.30
HS150	Calcite	29.344(2)	0.97-1.99	1.42	0.02-0.33	0.10	0.02-0.45	0.23
HS150 FRESH[2]	Calcite	29.314(2)	3.49-5.04	4.17	0.01-0.10	0.05	0.01-0.07	0.04
HS500	Calcite	29.301(2)	0.11-4.91	3.85	0.02-0.19	0.07	0.01-0.07	0.04
YSL	calcite, vaterite	29.352(2)	0.08-0.29	0.12	0.08-0.19	0.14	0.03-0.10	0.06
YSH	calcite, vaterite	29.352(2)	0.07-0.19	0.13	0.12-0.28	0.19	0.01-0.08	0.04

[a] values taken from Lee et al. (2008)

[b] FRESH refers to granules collected from earthworm depurate at the end of the experiment rather than those recovered from the bulk soil by sieving

Table 5. Table summarising XAS fits for the selected points on a granules produced by *L. terrestris* in HS100, YSL and YSH together with relevant standards

Point/Std	Notes	Scattering Atom	Coordination Number	Interatomic distance (Å)	Debye-Waller factor (Å^2)	Fit Index
Sr in HS100 Point A	High Sr in the centre of the granule	O	6	2.51(±0.02)	0.013(±0.002)	28.7
		C	6	3.38(±0.06)	0.040(±0.017)	
		Ca	6	4.09(±0.02)	0.024(±0.005)	
		Ca	6	5.04(±0.06)	0.032(±0.017)	
Sr in HS100 Point B	Low Sr on the edge of the granule	O	6	2.52(±0.01)	0.014(±0.002)	34.9
		C	6	3.35(±0.03)	0.030(±0.011)	
		Ca	6	4.10(±0.04)	0.029(±0.008)	
		Ca	6	5.04(±0.07)	0.027(±0.009)	
Sr in HS100 Point C	Medium Sr near a rim	O	6	2.51(±0.01)	0.012(±0.003)	31.5
		C	6	3.36(±0.06)	0.049(±0.027)	
		Ca	6	4.10(±0.04)	0.036(±0.065)	
		Ca	6	5.02(±0.07)	0.044(±0.022)	
Sr in YSL Point A	Medium Sr near the edge of the granule	O	6	2.50(±0.01)	0.013(±0.004)	39.5
		C	6	3.32(±0.08)	0.035(±0.025)	
		Ca	6	4.10(±0.06)	0.024(±0.007)	
		Ca	6	5.02(±0.14)	0.040(±0.028)	
Sr in YSH Point A	High Sr on a hotspot top left side of the granule	O	6	2.53(±0.02)	0.017(±0.004)	33.7
		C	6	3.29(±0.11)	0.030(±0.017)	
		Ca	6	4.08(±0.06)	0.037(±0.050)	
		Ca	6	5.01(±0.09)	0.034(±0.036)	
Sr adsorbed onto granule		O	6	2.52(±0.02)	0.008(±0.006)	33.0
		C	6	3.40(±0.19)	0.048(±0.082)	
		Ca	6	4.10(±0.07)	0.028(±0.017)	
		Ca	6	5.02(±0.06)	0.019(±0.027)	
Sr in YSH Point B	Medium Sr	O	8.2	2.55(±0.01)	0.025(±0.005)	29.3
		C	5.2	2.95(±0.10)	0.035(±0.025)	
		Ca	3.5	4.13(±0.06)	0.040(±0.019)	
Sr adsorbed onto calcite		O	6	2.51(±0.01)	0.010(±0.004)	31.7
		C	6	3.33(±0.11)	0.008(±0.017)	
		Ca	6	4.07(±0.03)	0.022(±0.010)	
		Ca	6	5.00(±0.04)	0.008(±0.007)	
Vaterite co-precipitated with Sr		O	8	2.55(±0.01)	0.022(±0.003)	23.8
		C	5.7	2.94(±0.15)	0.035(±0.022)	
		Ca	4.4	4.17(±0.04)	0.043(±0.014)	